

**Zeitschrift:** Schweizerische mineralogische und petrographische Mitteilungen =  
Bulletin suisse de minéralogie et pétrographie

**Band:** 63 (1983)

**Heft:** 1

**Artikel:** Alpine metamorphism of calcareous rocks along a cross-section in the  
Central Alps : occurrence and breakdown of muscovite, margarite and  
paragonite

**Autor:** Frank, Erik

**DOI:** <https://doi.org/10.5169/seals-48722>

### **Nutzungsbedingungen**

Die ETH-Bibliothek ist die Anbieterin der digitalisierten Zeitschriften auf E-Periodica. Sie besitzt keine Urheberrechte an den Zeitschriften und ist nicht verantwortlich für deren Inhalte. Die Rechte liegen in der Regel bei den Herausgebern beziehungsweise den externen Rechteinhabern. Das Veröffentlichen von Bildern in Print- und Online-Publikationen sowie auf Social Media-Kanälen oder Webseiten ist nur mit vorheriger Genehmigung der Rechteinhaber erlaubt. [Mehr erfahren](#)

### **Conditions d'utilisation**

L'ETH Library est le fournisseur des revues numérisées. Elle ne détient aucun droit d'auteur sur les revues et n'est pas responsable de leur contenu. En règle générale, les droits sont détenus par les éditeurs ou les détenteurs de droits externes. La reproduction d'images dans des publications imprimées ou en ligne ainsi que sur des canaux de médias sociaux ou des sites web n'est autorisée qu'avec l'accord préalable des détenteurs des droits. [En savoir plus](#)

### **Terms of use**

The ETH Library is the provider of the digitised journals. It does not own any copyrights to the journals and is not responsible for their content. The rights usually lie with the publishers or the external rights holders. Publishing images in print and online publications, as well as on social media channels or websites, is only permitted with the prior consent of the rights holders. [Find out more](#)

**Download PDF:** 03.05.2026

**ETH-Bibliothek Zürich, E-Periodica, <https://www.e-periodica.ch>**

# **Alpine metamorphism of calcareous rocks along a cross-section in the Central Alps: occurrence and breakdown of muscovite, margarite and paragonite**

by *Erik Frank\**

## **Abstract**

The effects of the progressive Alpine metamorphism on Mesozoic cover rocks (Bündnerschiefer, Calcescisti) were studied along a cross-section in the western Lepontine Alps between Brig (lower greenschist facies) and Crevola (higher amphibolite facies). Changes in the mineral assemblages of calcareous schists and silicious dolomites with respect to metamorphic grade are documented. Microprobe as well as some X-ray data are given for muscovite, margarite, paragonite, biotite, chlorite, garnet, calcic amphibole, clinozoisite-zoisite, plagioclase, K-feldspar, scapolite, staurolite, kyanite, corundum, graphite and calcite. Local assemblages, textural evidence and mineral composition data indicate that chemical equilibrium was not attained on the scale of a single thin section. Microprobe analyses show that chemical equilibrium is restricted to local domains of contacting grain boundaries. This phenomenon may be related to the differential uplift and cooling regime in this part of the Central Alps as documented by isotopic mineral ages. Nevertheless, a regular pattern of mineral assemblages could be observed and the following mineral zones and reaction-isograds could be mapped with increasing grade: first appearance of biotite + calcite, garnet and Ca-amphibole, respectively; paragonite + calcite + quartz-“out” isograd, margarite + calcite + quartz-“out” isograd, scapolite-“in” isograd, muscovite + calcite + quartz-“out” isograd. Therefore, the relative upper thermal stability limits of the three white micas muscovite, margarite and paragonite in the presence of calcite + quartz have been documented for the first time. Metamorphic conditions have been estimated using different calibrated geothermometers and geobarometers and by comparing the observed mineral assemblages with experimental data. Along the cross-section, P-T-data increase from 2–3 kb/400–420°C at Brig to 6–8 kb/580–620°C at Crevola.

## **Introduction**

The zones of regional Alpine metamorphism are well documented in the Central Alps showing a systematic concentric regional pattern (NIGGLI 1970).

---

\* Mineralogisch-Petrographisches Institut der Universität Basel, Bernoullistrasse 30, CH-4056 Basel, Switzerland and Mineralogisch-Petrographisches Institut der Universität Bern, Baltzerstrasse 1, CH-3012 Bern.

Present address: Swiss Federal Office of Energy, HSK, CH-5303 Würenlingen, Switzerland.

Pressure-temperature estimates, as deduced from critical mineral assemblages in pelites, impure dolomites and ultramafic rocks, indicate a general increase in metamorphic grade going from the north to the south (NIGGLI 1970, NIGGLI and NIGGLI 1965, CHATTERJEE 1961, WENK 1962, 1969, TROMMSDORFF 1966 and FREY 1969, 1974). The zone of highest metamorphic grade occurs in the Ticino area, the deepest tectonic unit in the Alps.

The present investigation reports the results of a mineralogical study on Mesozoic cover rocks (Bündnerschiefer) collected along a cross-section of increasing metamorphic grade from Brig to Verampio-Crevola (Italy). The aim of this work is (a) to present a regional distribution map of important minerals in calcareous mica-schists and marbles, (b) to provide further chemical data on these minerals, (c) to deduce the possible mineral reactions and (d) to estimate the P-T-conditions of the Alpine metamorphism.

### Geological setting

The study area lies in the western part of the Lepontine Alps (Fig. 1) within the lower units of the Pennine nappes. The nappe pile consists mainly of sheets

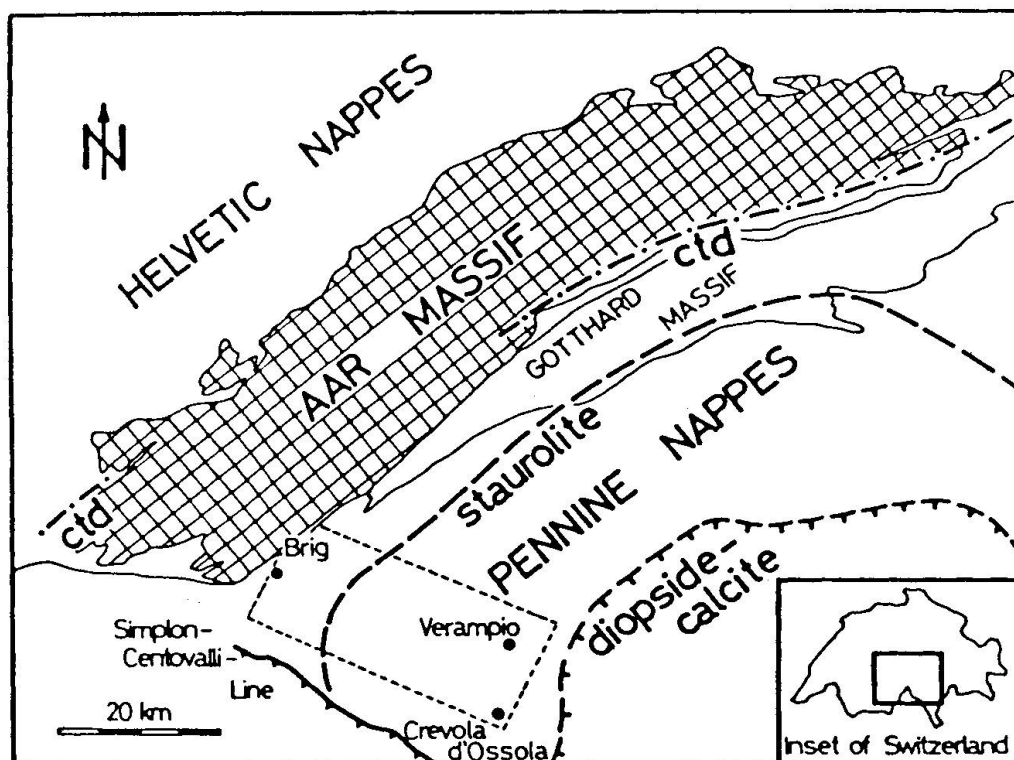


Fig. 1 Tectonic sketch map of the Central Alps and the location of the study area. Alpine metamorphic mineral zone boundaries are according to FREY and WIELAND (1978), NIGGLI and NIGGLI (1965) and TROMMSDORFF (1966) referring to the first appearance of chloritoid (ctd), staurolite and diopside-calcite respectively.

of polymetamorphic crystalline basement rocks including granitic and quartzofeldspathic gneisses, paraschists and amphibolites, separated from each other by Mesozoic cover rocks (calcareous schists, marbles, dolomites, quartzites, pelites). The different basement sheets represent old continental crust on which the Mesozoic cover rocks were deposited. These sediments were affected by only the Alpine orogeny and are therefore well suited for a study of the Alpine metamorphic history. According to a number of recent investigations it is now well established that the Alpine orogeny had at least two distinct phases (BEARTH 1958, VAN DER PLAS 1959, NIGGLI 1970, JAEGER 1973, ERNST 1973, FREY et al. 1974 and TRÜMPY 1960, 1980): an Eo-Alpine high-pressure event of late Cretaceous age, followed by a high-temperature regime during Mid-Tertiary time. However, in the high-grade part of the Central Alps (Leptontine area) no petrological or geochronological evidence of an Eo-Alpine high-pressure metamorphism has been found so far. If such an event took place in this area all characteristic mineral assemblages have been completely overprinted by subsequent high-temperature recrystallization. Detailed structural work indicates that there are at least three different stages of folding in this area (CHATTERJEE 1961, HALL 1972, MILNES 1973, 1974, AYRTON and RAMSAY 1974 and STECK et al. 1979). According to HALL (1972) and MILNES (1973) one of the most important structural features is that an already interleaved basement-cover pile was later subjected to intense isoclinal folding on a large scale. These isoclinal folds can be subdivided into main Alpine folds, developed before or during the rise in temperature, and late Alpine folds formed during the period of high temperatures. The growth of most porphyroblasts such as garnet, staurolite and kyanite took place after the formation of the main schistosity between the second and third phase of deformation ( $D_2$  and  $D_3$ , AYRTON and RAMSAY 1974). However, recrystallization also tends to outlast deformation processes as can be observed most clearly on plagioclase textures or from reaction textures (FRANK 1979).

#### Mineral distribution

This study was confined to mapping and examining the mineral assemblages in calcareous rocks, which are rather consistently exposed along the cross-section from Brig to Crevola (Fig. 2). Metamorphic grade generally increases from northwest to southeast, from the chlorite zone to the higher staurolite zone (CHATTERJEE 1961, STRECKEISEN + WENK 1974).

#### CALCAREOUS MICA-SCHISTS

The occurrence and the regional distribution of relevant minerals are summarized in Fig. 3. In the low-grade samples muscovite, chlorite, calcite and

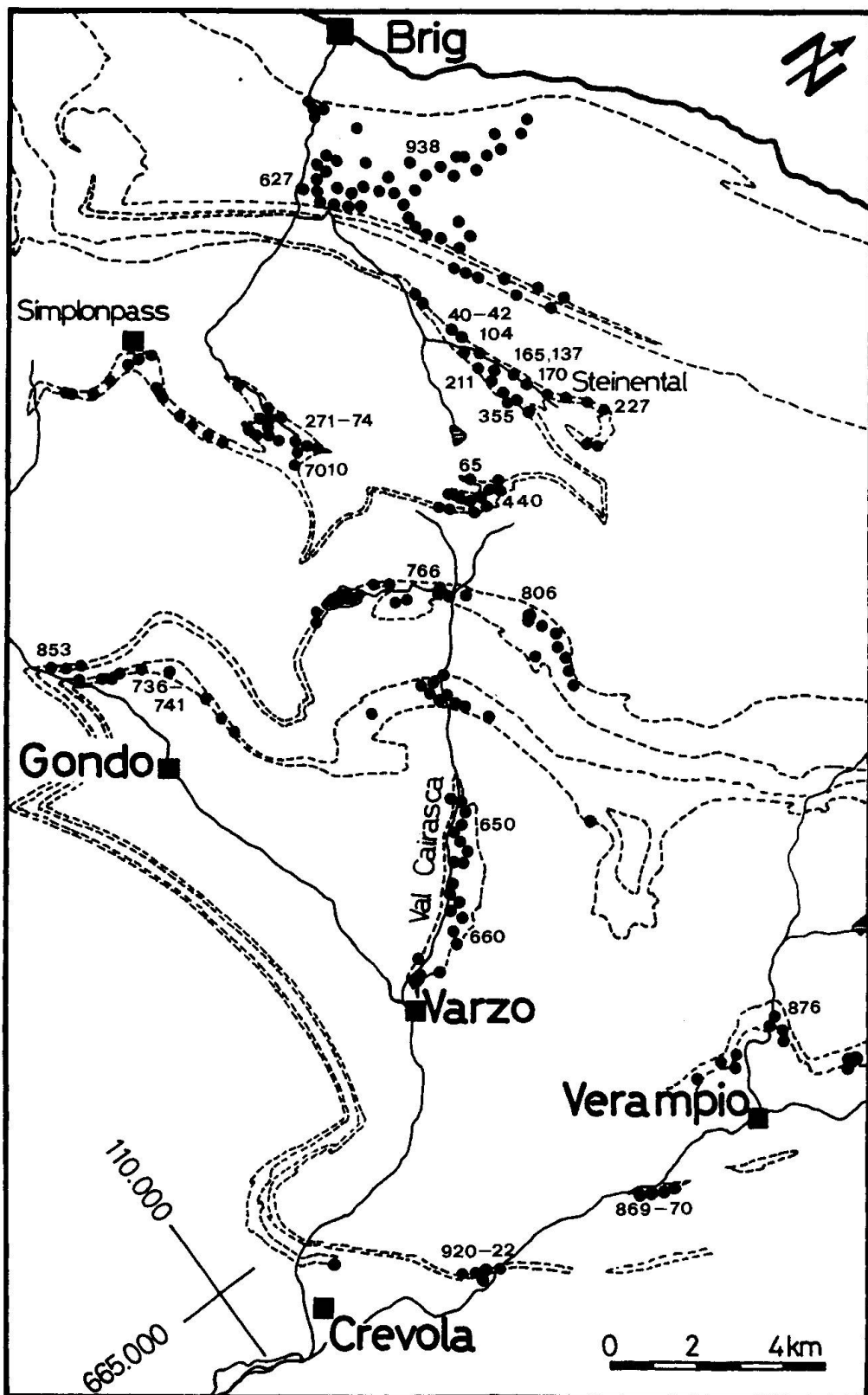
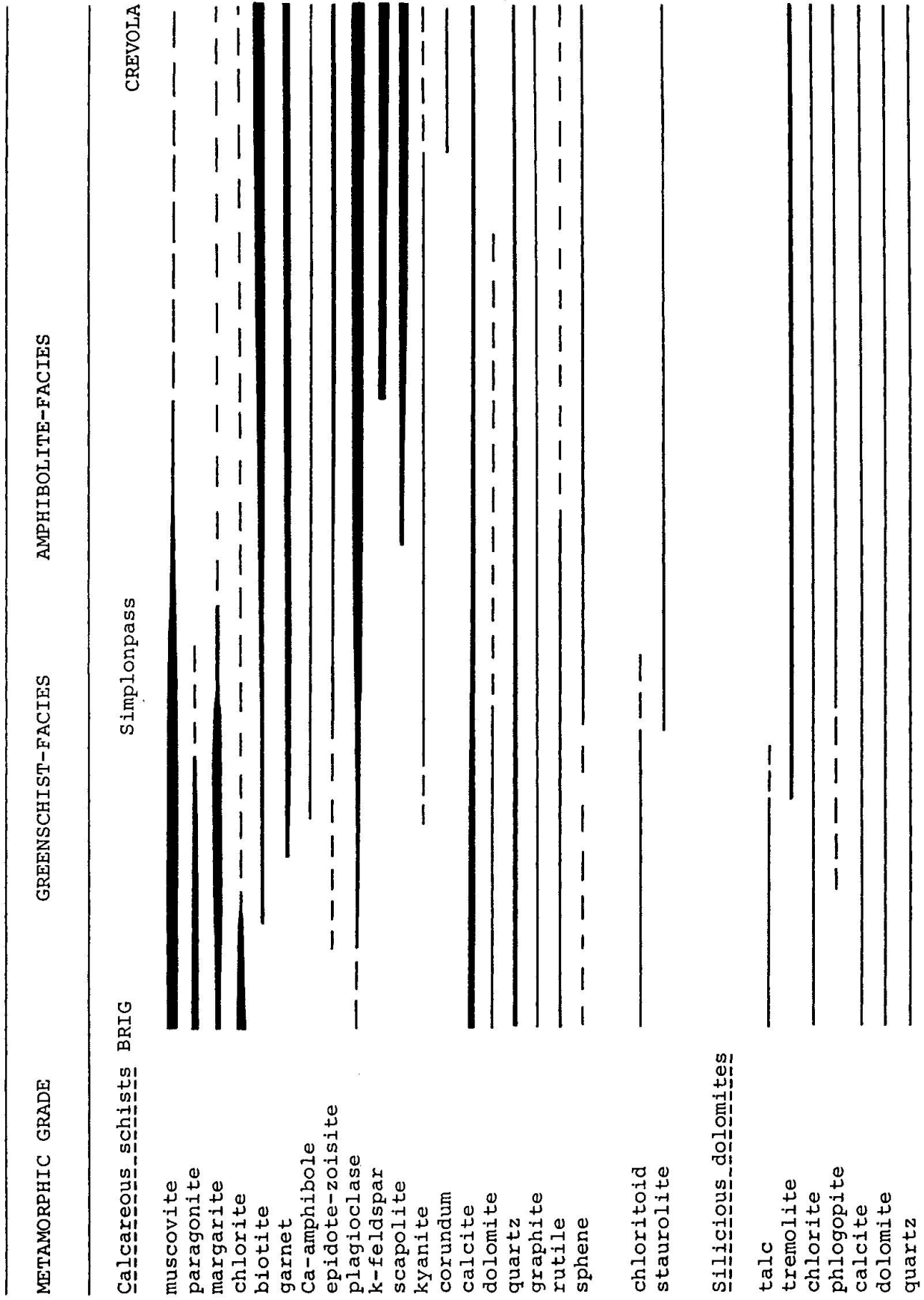


Fig. 2 Outline map of the cross section Brig-Crevola showing principle locations. Countours indicate the regional occurrence of Mesozoic cover rocks, separating the crystalline basement rocks. Sample numbers refer to the specimens which were analyzed by electron microprobe technique.

Fig. 3 Distribution pattern of the most important minerals in Mesozoic cover rocks along the cross section Brig-Crevola.



quartz are the dominant matrix minerals. Furthermore, in many samples paragonite and margarite are also present. To date margarite has been described in only a few localities in the Central Alps (FREY + NIGGLI 1972, FOX 1975), but recent studies show margarite to be quite common in metamorphic rocks in the Alps (FREY et al. 1982). The lowest grade biotite-calcite assemblages occur about 3 km south from Brig, where a continuous formation at the expense of chlorite and muscovite may be assumed. The next phases entering the progressive sequence are almandine-rich garnet and calcic amphibole. Proceeding further to the south into amphibolite-facies conditions as defined by the first appearance of staurolite + kyanite in pelitic rocks, the following two additional phases can be recognized: first appearance of meionitic scapolite and of monoclinic k-feldspar. The assemblage k-feldspar-anorthite indicates the breakdown of the assemblage muscovite-calcite-quartz, whereas scapolite was formed at the expense of calcite + anorthite-rich plagioclase. Generally one observes in all high-grade samples a substantial increase in modal plagioclase content which is related to various breakdown reactions of muscovite, paragonite and margarite producing plagioclase. In these rocks biotite is much more abundant than the white micas and is the dominant sheet-silicate mineral. In few high-grade samples from the Verampio-Crevola area the unusual assemblage anorthite-corundum can be found. Local occurrence of epidote-zoisite minerals is very common in most samples. Zoisite predominantly occurs in the high-grade specimens. Important accessory minerals are graphite (present in all samples), rutile and sphene as well as pyrrhotite, pyrite and/or ilmenite.

#### IMPURE DOLOMITES

Silicious dolomites are not much abundant in the studied area. In these rocks the first appearance of tremolite can be observed in the Steinental and is characterized by the five-phase assemblage talc-tremolite-dolomite-calcite-quartz. Note that this assemblage already occurs below the staurolite-isograd at obviously lower temperature conditions. The isochemical high-grade assemblage diopside-calcite has not been observed.

#### METAPELITES

Monoclinic chloritoid as well as staurolite are found only in rocks of aluminium-rich bulk composition (pelitic layers). Both minerals are quite common in upper Triassic phyllites (Quartenschiefer) in this area.

### Mineral chemistry

For this study some 300 rock samples were examined microscopically. Thin sections were stained for carbonate minerals and for k-feldspar using the technique of EVENY, + SHERMAN (1962) and BAILEY + STEVENS (1960). Separated mica fractions were analyzed by X-ray diffractometry and Guinier-camera techniques. Minerals in 28 polished thin sections were analyzed by an ARL-SEMQ electron microprobe combined with a Tracor-Northern energy dispersive detector system. The microprobe was operating at an acceleration voltage of 15 kV and a sample current of 15 nA. To minimize drift effects counting time was controlled by means of beam current integration. For standardization natural and synthetic minerals were used. Data reduction was performed by a BENCE-ALBEE type matrix correction program. Additional analytical details are given by SCHWANDER + GLOOR (1980). From replicate analyses the precision of the data is on the order of 0.6–1.5 relative percent for high concentrations and on the order of 5 to 10 percent for concentrations less than one weight percent. In table 1 the mineral assemblages of the samples used for microprobe analyses are summarized. Representative mineral analyses spanning a range of grade are given in the appendix (cf. tables 2–13).

#### WHITE MICAS (MUSCOVITE, MARGARITE, PARAGONITE)

The white micas muscovite, margarite and paragonite were routinely identified by X-ray technique using the criteria described by VELDE (1971), CHATTER-

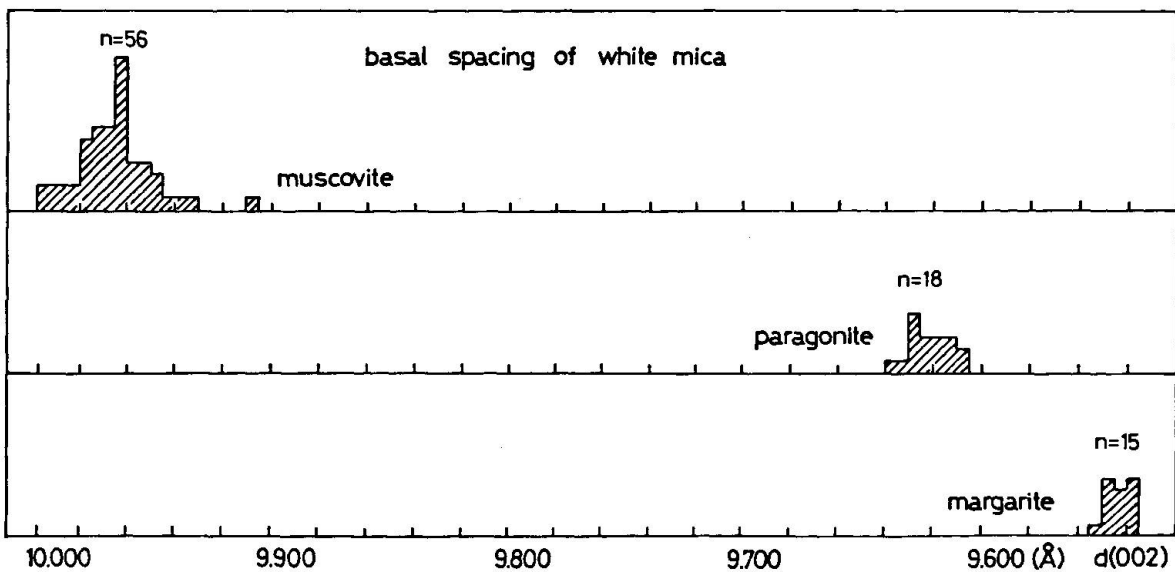


Fig. 4 Frequency distribution of white mica basal spacing values  $d(002)$ .

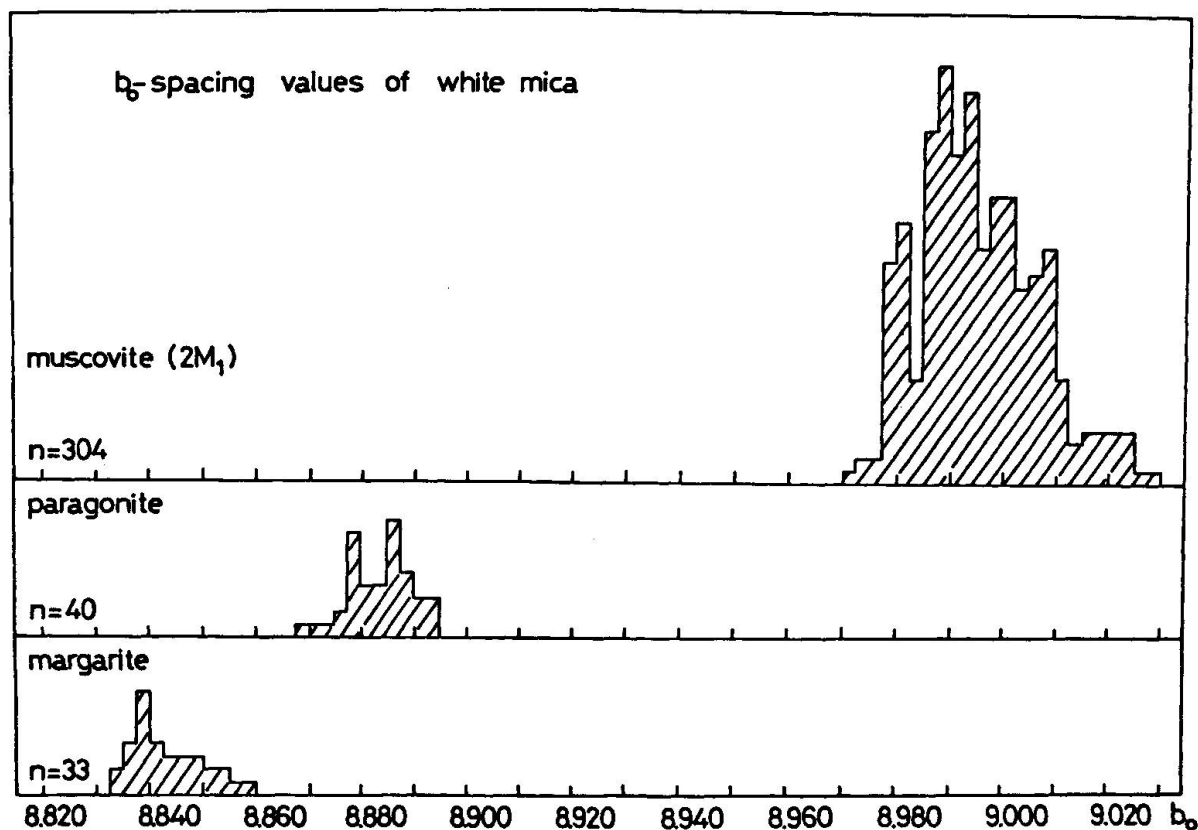


Fig. 5 Frequency distribution of white mica  $b_0$ -spacing values.

JEE (1974) and GUIDOTTI + SASSI (1974). When grain size permitted, microprobe analyses were also done. Muscovite, margarite and paragonite can be easily distinguished from each other by their  $d(002)$  and  $b_0$ -spacing values as shown in figures 4 and 5. Their characteristic frequency distribution pattern reveal some significant broad scatter which points to differences in their solid-solution behaviour. Muscovite (002) basal spacing values for example range from 9.999 Å to 9.905 Å. This shift to lower values suggests a substantial solid-solution of paragonite into muscovite, ranging up to 30 mole percent paragonite according to calibrated regression curves given in the literature (GUIDOTTI + SASSI 1974). By plotting against each other the basal-spacings of coexisting muscovite and paragonite (Fig. 6), some linear correlations can be found for these samples which fit quite well the regression line determined by ZEN + ALBEE (1964) for the muscovite-paragonite solid-solution. In this case, a significant deviation from the regression line can be observed if margarite is present in addition (Fig. 6, open symbols), indicating mainly a reduction of the paragonite basal spacing. This shift is due to some solid-solution of margarite-component into paragonite.

Examination of white mica polytype by Guinier-camera films reveals that all samples are of the  $2M_1$  type (BORG + SMITH 1974). Microprobe analyses of mus-

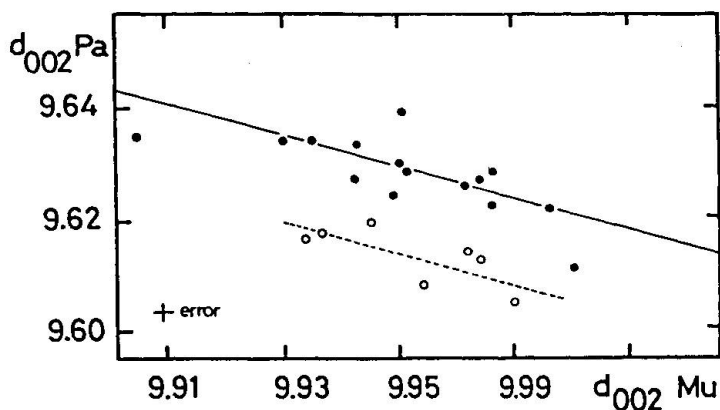


Fig. 6 Basal spacing values of coexisting muscovite and paragonite. The straight line refers to the regression curve of ZEN and ALBEE (1964). Open symbols indicate the presence of margarite in addition.

covite are shown in figure 7. All data are calculated on the basis of 22 oxygens per formula unit (Table 2). Fe is considered to be in the divalent state, an assumption which may be justified because of the presence of graphite and the absence of haematite in our samples. The results plotted in terms of Si-Al-(Fe + Mg) proportions indicate a slight variation from ideal muscovite to phengitic compositions. Tetrahedral Si increases from 6.0 up to 6.56 atoms per formula unit. The  $Al^{VI}$ -Fe-Mg diagram clearly shows the substitutional trend of octahedral sites pointing to a tschermaks type of exchange  $Al^{IV}Al^{VI}Si_{-1}(Fe, Mg)_{-1}$ . This behaviour is confirmed if the results are plotted on a Si- $Al^{IV}Al^{VI}$  diagram (Fig. 8), and indicates a strong Si-Al correlation. This diagram furthermore allows an estimation to be made of the divalent/trivalent state of iron in the sam-

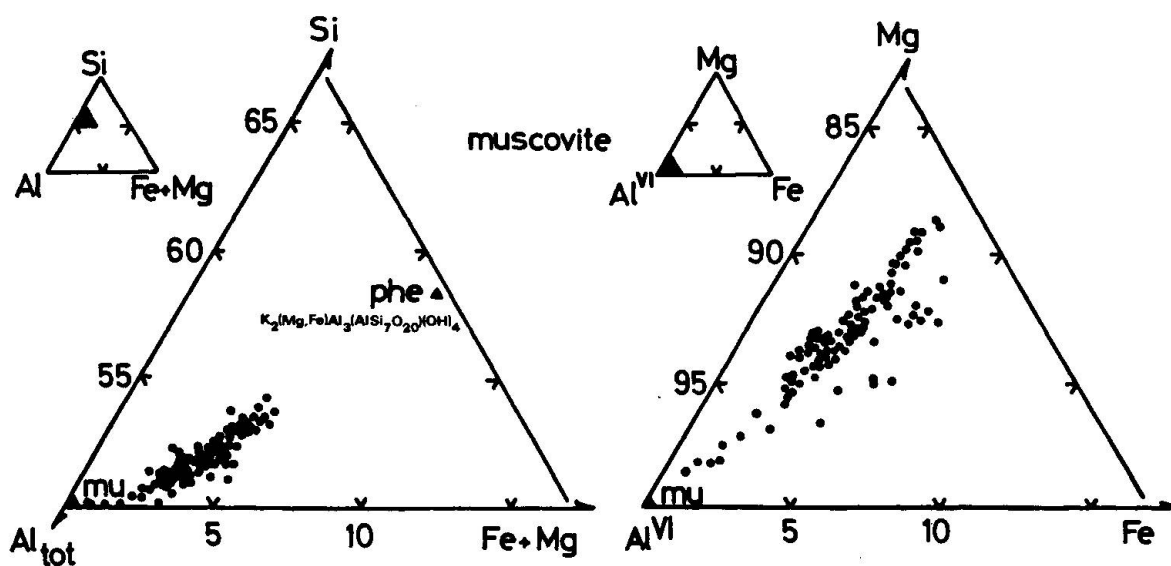


Fig. 7 Variation of muscovite composition in a Si-Al-(Fe+Mg) and a  $Al^{VI}$ -Mg-Fe-projection.

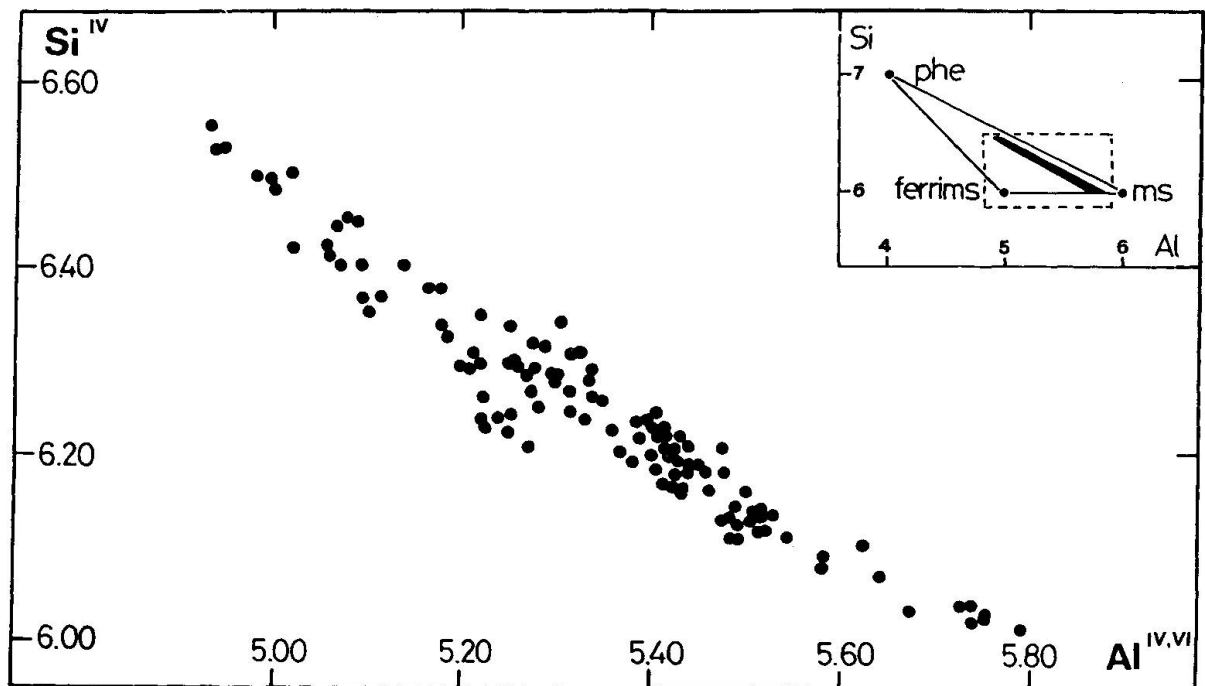


Fig. 8 Correlation of tetrahedral Si versus total Al with respect to the endmembers muscovite, ferrimuscovite and phengite.

ples by comparing these data to the theoretical ferrimuscovite-, celadonite- and muscovite-endmember compositions. These data correlate very closely with the muscovite-phengite join (phengite is defined here as a species intermediate between muscovite and celadonite) suggesting that ferrimuscovite solid-solutions must be very limited. The amount of paragonite component present in these muscovites (Fig. 9) increases up to 26 mole percent paragonite. This is consistent with the estimations made from the X-ray data. No significant margarite component was detected in the muscovites. From figure 9 there seems to be some trend to a deficiency of interlayer cations with increasing  $KNa_{-1}$  substitution. The presence of small amounts of Ba causing this trend deviation cannot be excluded because of the poor resolution of this element by electron microprobe technique (the detection limit is on the order of 0.15 weight percent BaO because of interference with the Ti-spectrum). As a function of increasing metamorphic grade the following compositional changes can be deduced along the cross-section (Fig. 10). All samples show characteristic variations of octahedral Fe, Mg and Al and of tetrahedral Si and Al. The corresponding frequency distribution of Si indicates a general positive trend towards Al-rich muscovite with increasing grade. From these data we suggest that in many samples the mineral assemblages are not limited ones in respect to Al-Si-Fe-Mg exchange. On the other hand a significant correlation of Na/Na+K with respect to metamorphic grade can be observed (Fig. 10). In the lower grade samples, muscovites, often

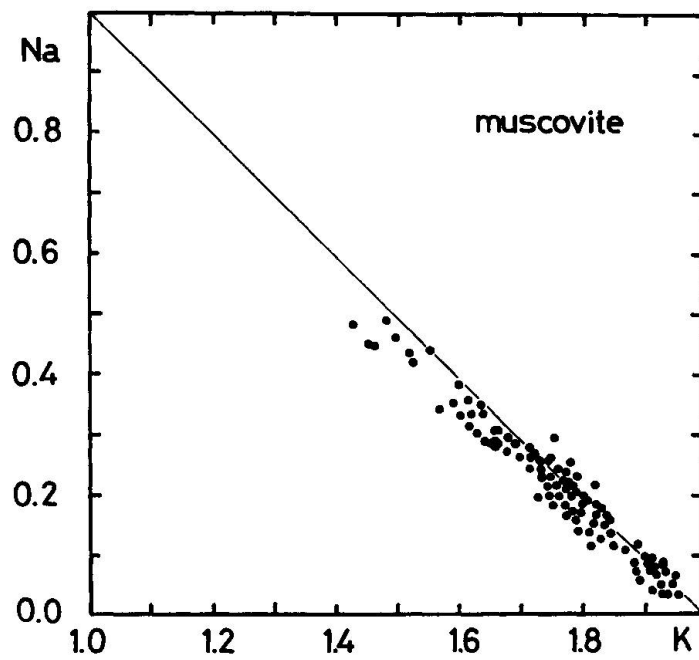


Fig. 9 Na-K correlation diagram of muscovite.

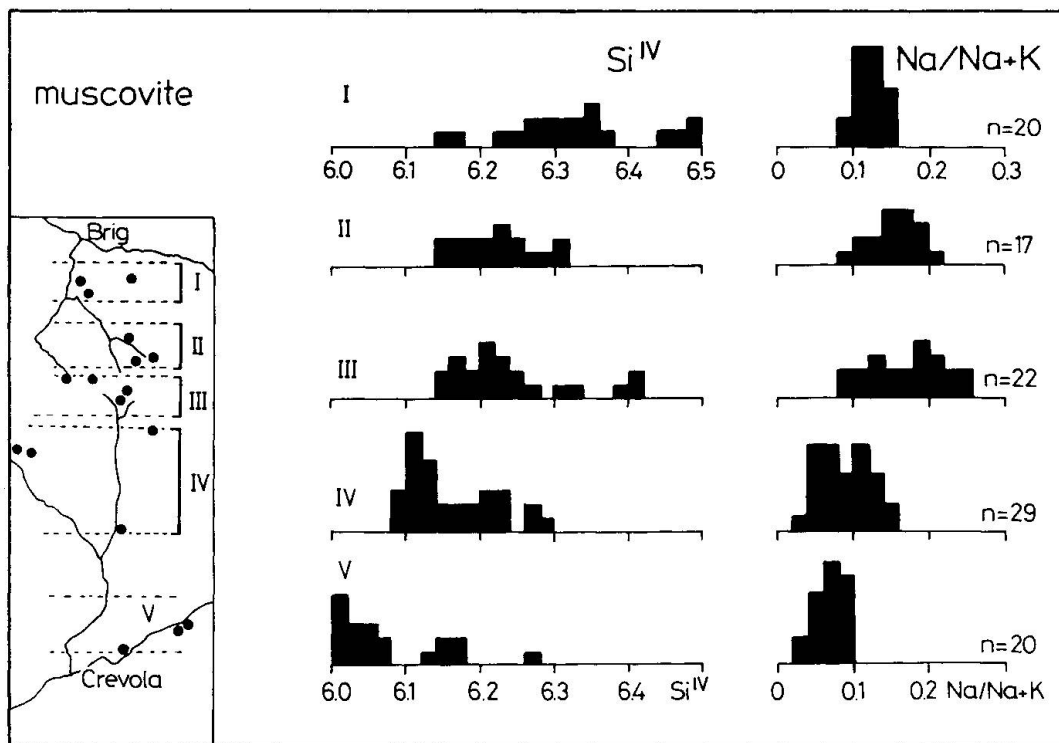


Fig. 10 Regional variation of muscovite composition as a function of increasing metamorphic grade: variation of  $\text{Si}^{\text{IV}}$  and  $\text{Na}/\text{Na}+\text{K}$ .

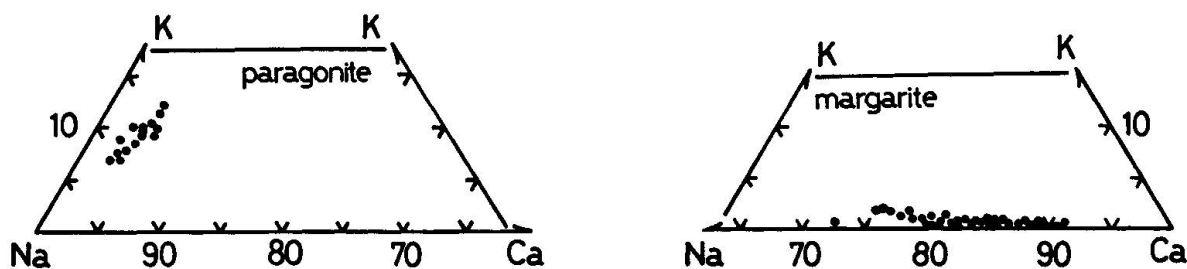


Fig. 11 Composition of margarite and paragonite in terms of Na-Ca-K proportions.

coexisting with paragonite, show increasing Na/Na+K ratios ranging from about 0.10 up to 0.26 with increasing grade (zone I, II and III in Fig. 10). At higher grade, the Na/Na+K ratios substantially decrease to less than 0.10. These observations are consistent with experimental and calculated muscovite-paragonite phase relations (THOMPSON 1974). Within one single thin section variable Na/Na+K ratios are found depending on whether other Na-bearing phases are present in mutual contact with muscovite (for example paragonite). This points to a Na-K exchange in local domains.

The composition of margarite and paragonite is shown in Fig. 11 in terms of K-Na-Ca endmembers. Margarite analyses plot very close to the Ca-Na join indicating an extended solubility of paragonite component, whereas the muscovite component seems to be negligible. On the other hand analytical data of paragonite show that there is an appreciable replacement of Na by both K and Ca. Octahedral sites of both margarite and paragonite are occupied by only minor amounts of Fe and Mg (0.1–0.8 wt.% FeO, 0.1–0.3 wt.% MgO) suggesting that there is very little or no phengite substitution in these mica.

#### BIOTITE

Representative analyses of biotites are plotted in Fig. 12. Anhydrous totals were calculated on the basis of 22 oxygens per formula unit. The biotite are found to be intermediate between Mg and Fe endmembers. Some deviation from ideal trioctahedral stoichiometry can be observed, the total number of ions in the octahedral sites being consistently lower than 6.0. This is probably due to a coupled substitution of octahedral (Mg, Fe)<sup>2+</sup> by Al<sup>3+</sup>, combined by some substitution of tetrahedral sites for maintaining the charge balance. Significant variations in Mg/Mg+Fe ratios can be observed in all biotites (Fig. 12). On a thin section the following systematics were found (Fig. 13): biotite isolated in the rock-matrix show Mg-richer compositions when compared

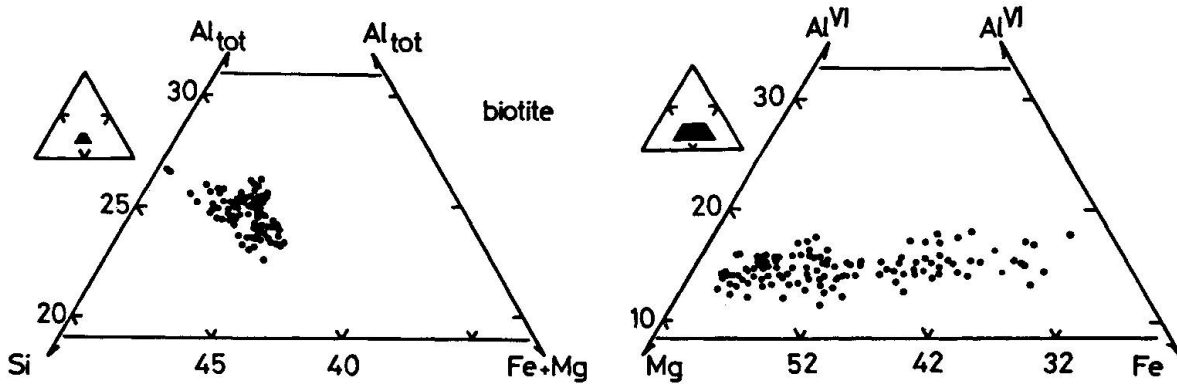


Fig. 12 Variation of biotite composition in terms of Al-Si-(Fe+Mg) and Al<sup>VI</sup>-Mg-Fe proportions.

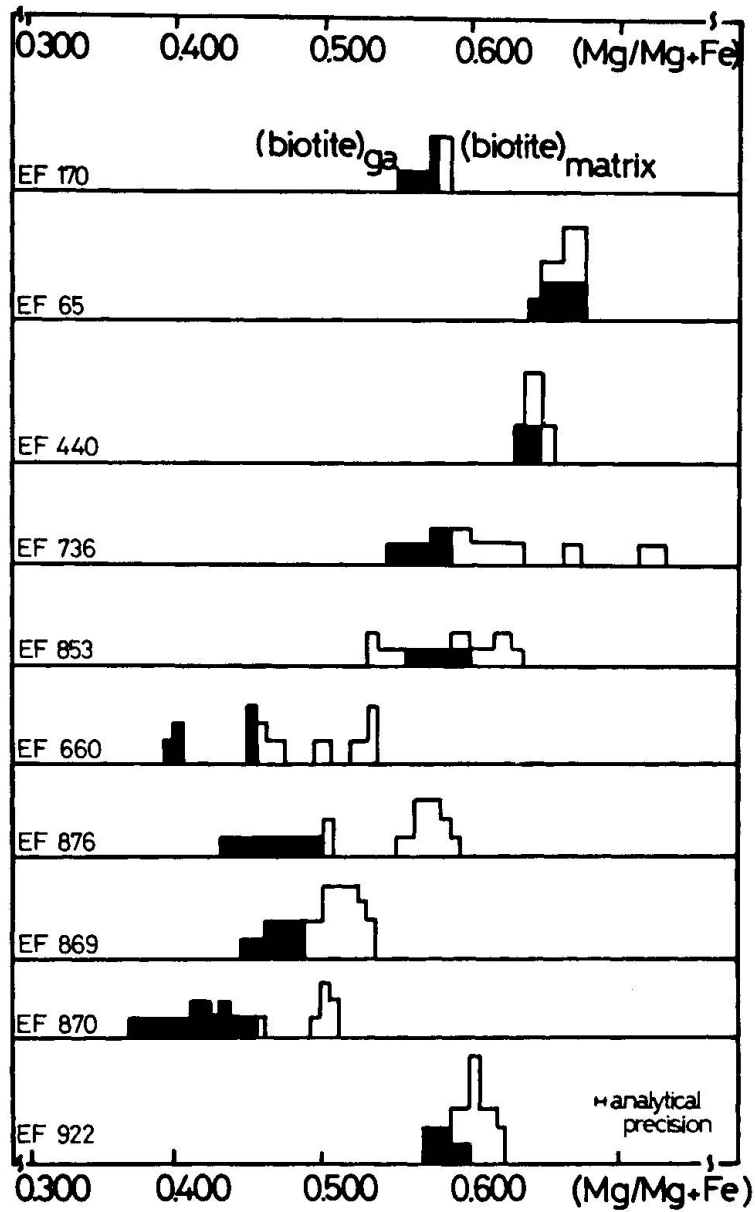


Fig. 13 Mg/Mg+Fe frequency distribution pattern for biotite along the metamorphic profile. Black area represents biotite in textural contact to garnet comparing to isolated biotites in the rock matrix.

to biotites in contact with garnets. These biotites are distinctly enriched in Fe. With increasing metamorphic grade biotites tend to become richer in Fe.

Considerable amounts of Ti are present in the biotites (up to 3.40 wt. %  $\text{TiO}_2$ ). Several substitutions are possible to account these high values of Ti. The most probable one is a coupled substitution of the type  $3\text{Al}^{\text{VI}}2\text{Al}^{\text{IV}} = 3\text{TiSi}$  (Fig. 14). A positive correlation of Ti-content to metamorphic grade is also observed (Fig. 15) with values of Ti increasing from 0.2 (at. prop.) in the north to 0.4 (at. prop) in the south. Similar behaviour of Ti in biotites has been described by KWAK (1968), EVANS + GUIDOTTI (1966) and GUIDOTTI (1970). Since all samples are probably  $\text{TiO}_2$ -saturated as evidenced by the presence of rutile and/or sphene, the increase in Ti with increasing grade suggests a temperature-dependent change of the Ti-saturation limit in biotite as described by KWAK (1968). Comparing Fig. 13 and Fig. 15 some possible correlations between Ti and  $\text{Mg}/\text{Mg}+\text{Fe}$  are evident, the values trending to lower  $\text{Mg}/\text{Mg}+\text{Fe}$  values with increasing Ti-content. A similar dependency was reported by DAHL (1970) and DALLMEYER (1974) who argued that the Ti-content directly controlled the  $\text{Mg}/\text{Mg}+\text{Fe}$  ratio in biotite.

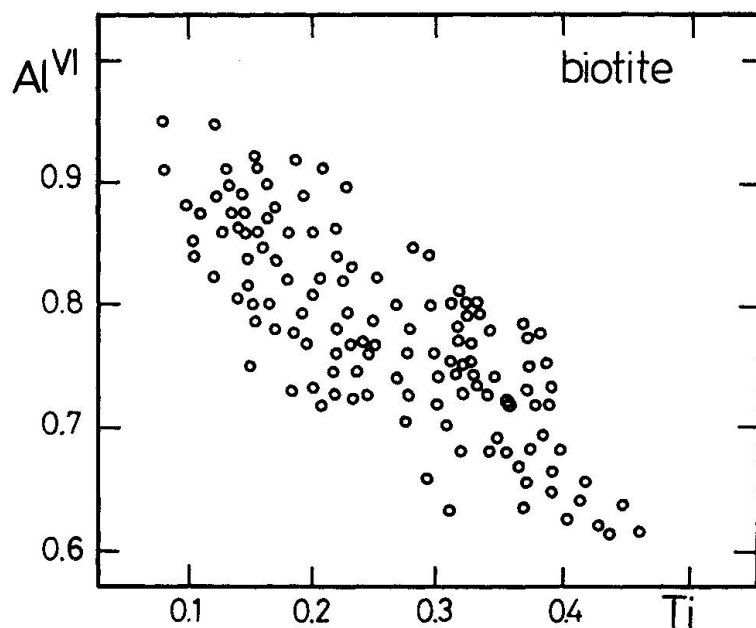


Fig. 14 Variation of octahedral Al and Ti in biotite.

#### CHLORITE

Analyses of chlorite are plotted in Fig. 16 using the classification scheme of HEY (1954). Structural formulae have been calculated on the basis of 28 oxygens and by assuming the tetrahedral sites are completely filled by Si and Al.

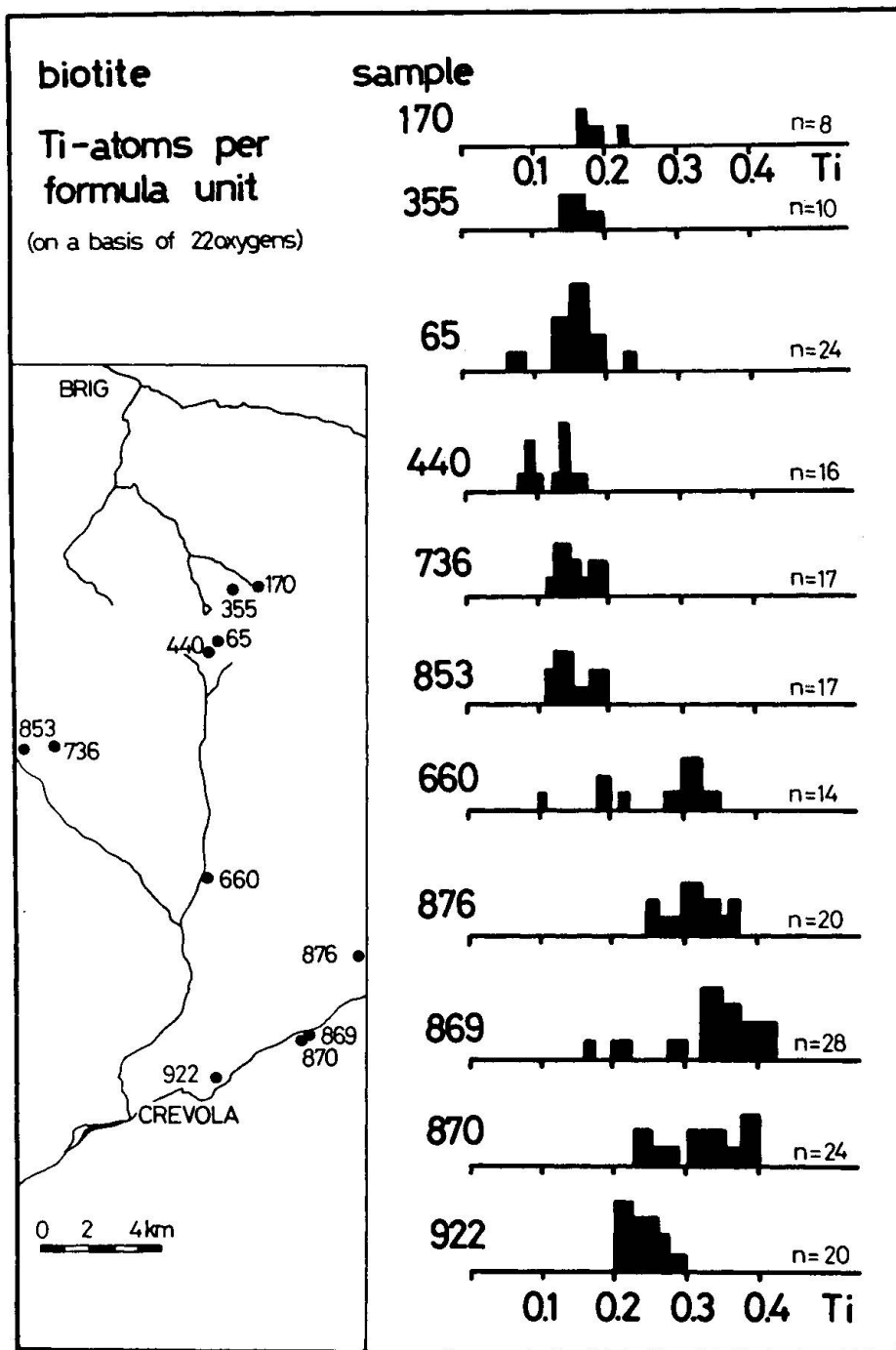


Fig. 15 Variation of Ti-content in biotite as a function of increasing metamorphic grade.

The compositions are predominantly ripidolite showing a wide range in the Fe/Fe+Mg ratios. The chlorites show a restricted range in Si from 5.1 to 5.7. In some samples minor amounts of MnO were detected (0.10–0.36 wt. %). Coexisting biotite and muscovite revealed no Mn suggesting that Mn preferentially enters the chlorite lattice. Retrograde chlorite typically has Fe-rich compositions.

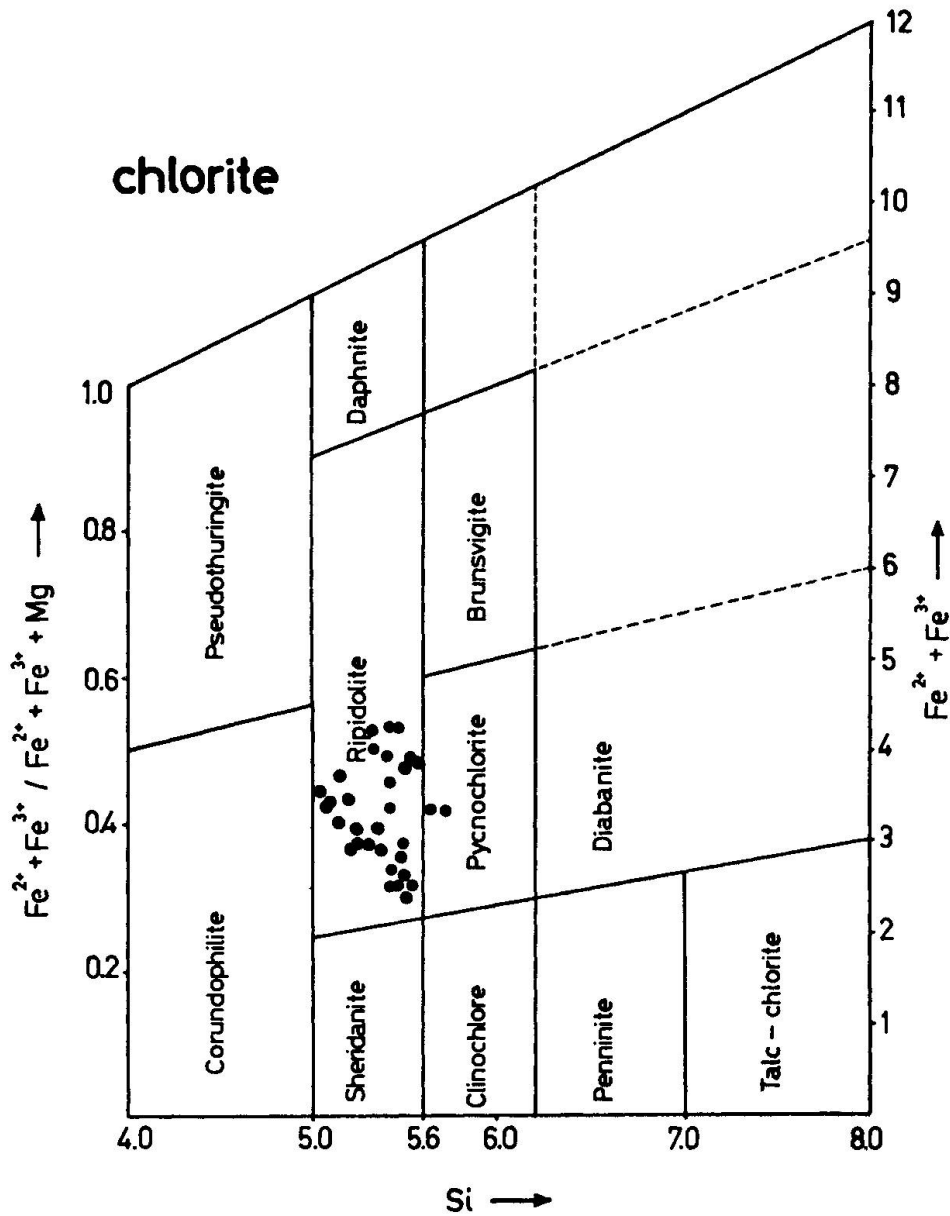


Fig. 16 Composition of chlorite plotted in the classification diagram of HEY (1954).

#### GARNET

Microprobe analyses of garnet were calculated on the basis of 24 oxygens per formula unit and assuming all iron to be in the divalent state. All garnets are chemically zoned with respect to Fe, Mn, Ca and Mg, whereas Al and Si are found to be relatively constant. Garnet compositions are plotted in Fig. 17 in terms of almandine, pyrope, grossular and spessartine endmembers, showing the core and rim compositions of the individual grains. The analyses reveal high almandine components in the range of 55 to 70 mole percent. All samples

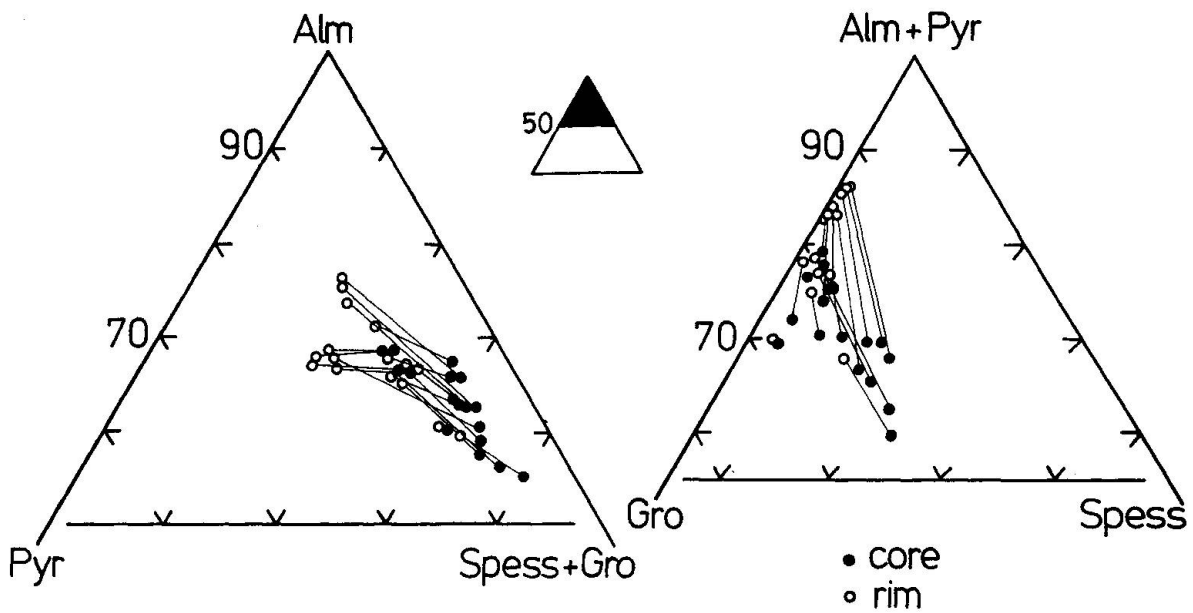


Fig. 17 Garnet composition in terms of almandine, pyrope, grossular and spessartine component. The lines join composition of core and rim of individual garnet porphyroblasts.

show the “normal” prograde bell-shape zoning patterns with cores enriched in Mn and Ca and depleted in Fe and Mg relative to their rims (Fig. 18). As a function of metamorphic grade a regional modification of this zoning pattern has been recognized. It is characterized by a systematic flattening of the MnO and the opposing FeO-curves and by a general decrease of the MnO-content with increasing grade. In all samples, the MgO-zoning remains on the same order of magnitude. Superimposed on these prograde zoning patterns garnet-rim compositions of some high-grade samples (EF 741) are modified showing Mg/Fe gradients within the last 50–100  $\mu\text{m}$ , which may be related to local Fe–Mg exchange reactions with coexisting minerals such as biotite or muscovite.

#### CALCIC AMPHIBOLE

In Fig. 19 and Fig. 20 the analytical results for calcic amphiboles are plotted. The samples show rather high Al-contents, ranging up to 18.2 wt.%  $\text{Al}_2\text{O}_3$ , suggesting a tschermakitic-pargasitic composition. No chemical zoning could be detected within individual grains. CaO, FeO and MgO are fairly constant in the range of about 11–12%, 15–18% and 8–9% respectively.  $\text{TiO}_2$ -contents were typically between 0.1–0.5 wt.%. In the silicious dolomites, tremolitic amphibole could be found containing substantial amounts of Al (up to 6.0 wt.%  $\text{Al}_2\text{O}_3$ ). The fluorine content is very low and often falls below the analytical detection limit of 0.2 wt.%.

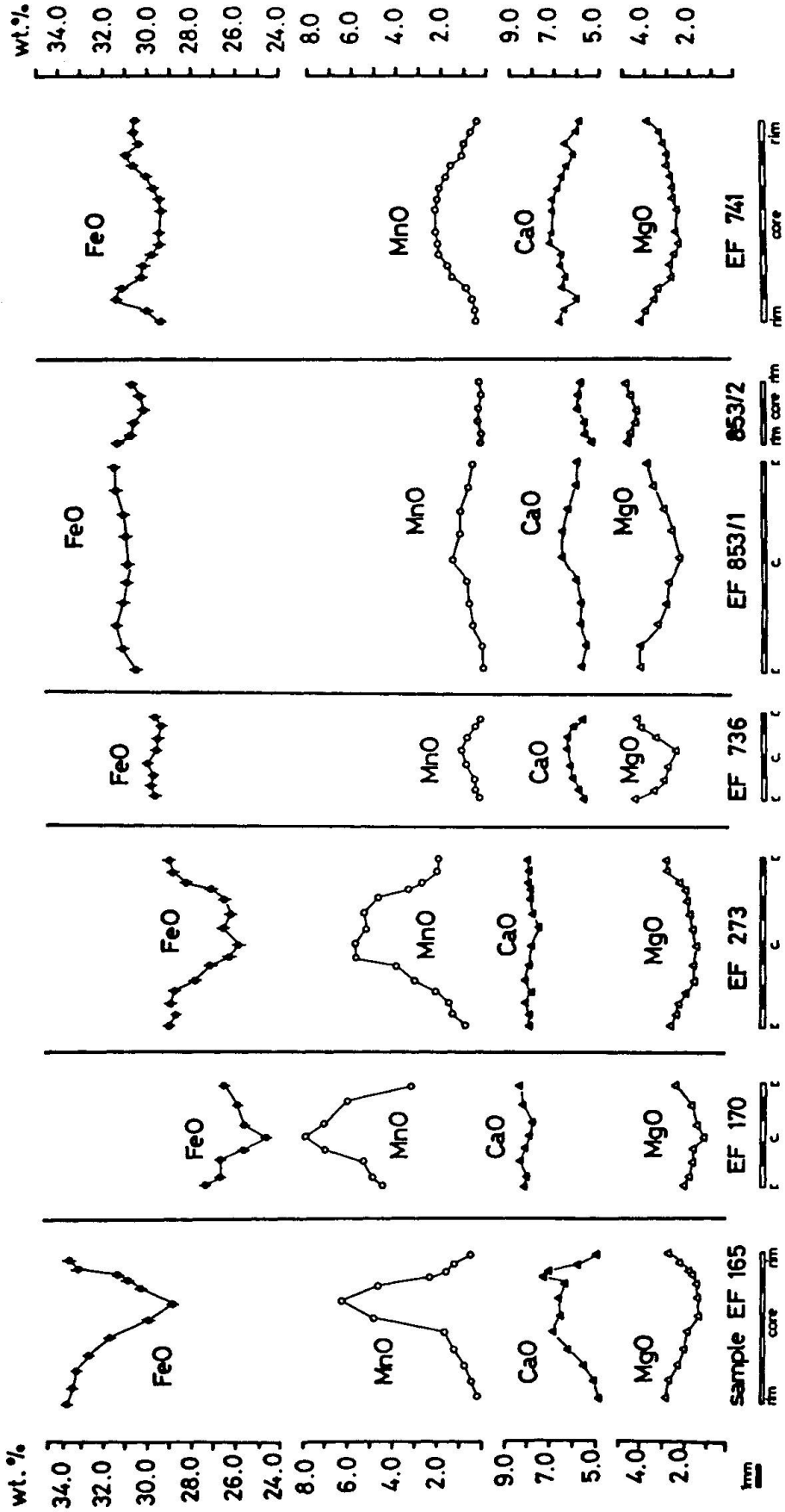


Fig. 18 Modification of garnet zoning patterns, plotted as a function of increasing metamorphic grade from left to right.

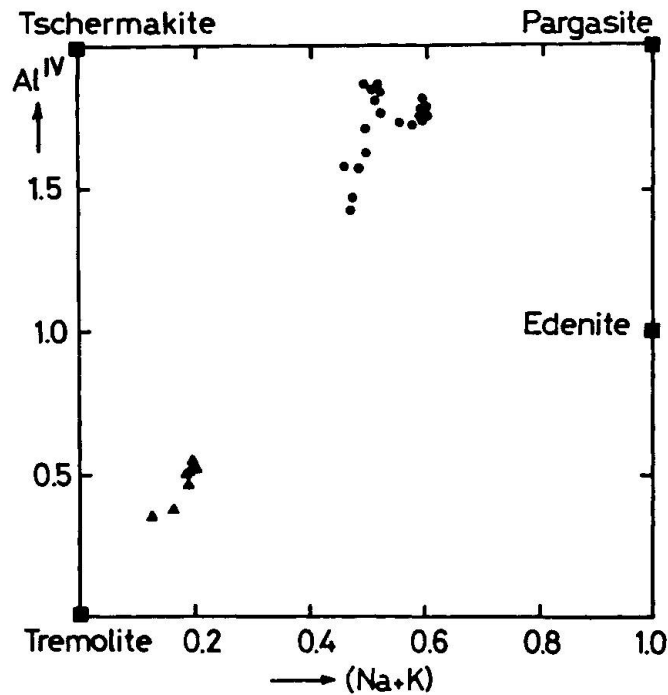


Fig. 19 Compositional variation of Ca-amphibole plotted in a  $Al^{IV}$ -(Na+K) diagram. Filled circles refer to calcareous rocks, triangles to dolomitic marbles.

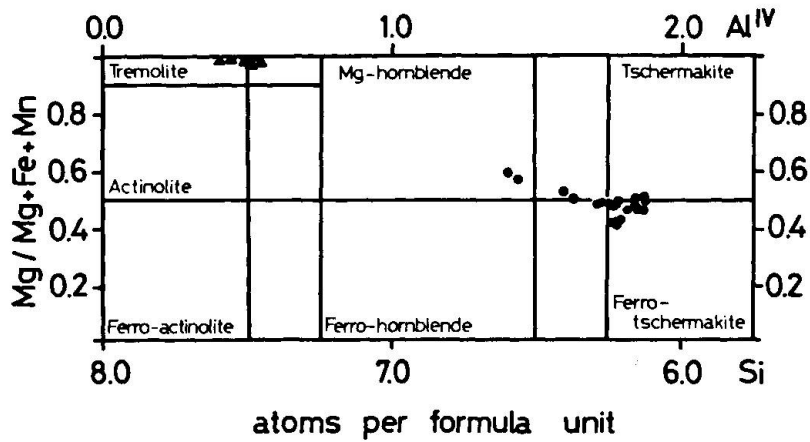


Fig. 20 Ca-amphibole composition shown in a LEAK type classification diagram. Same symbols as in Fig. 19.

#### CLINOZOISITE-ZOISITE

Microprobe analyses of clinozoisite-zoisite solid-solutions are shown in Fig. 21. All FeO was calculated as ferric. Octahedral aluminium and ferric iron exhibit a good reciprocal relationship. Lowgrade samples tend to be enriched in  $Fe^{3+}$  relative to  $Al^{VI}$ , hence are predominantly clinozoisitic. Some grains show distinct compositional zoning, with cores being richer in  $Fe^{3+}$  than rims. In the

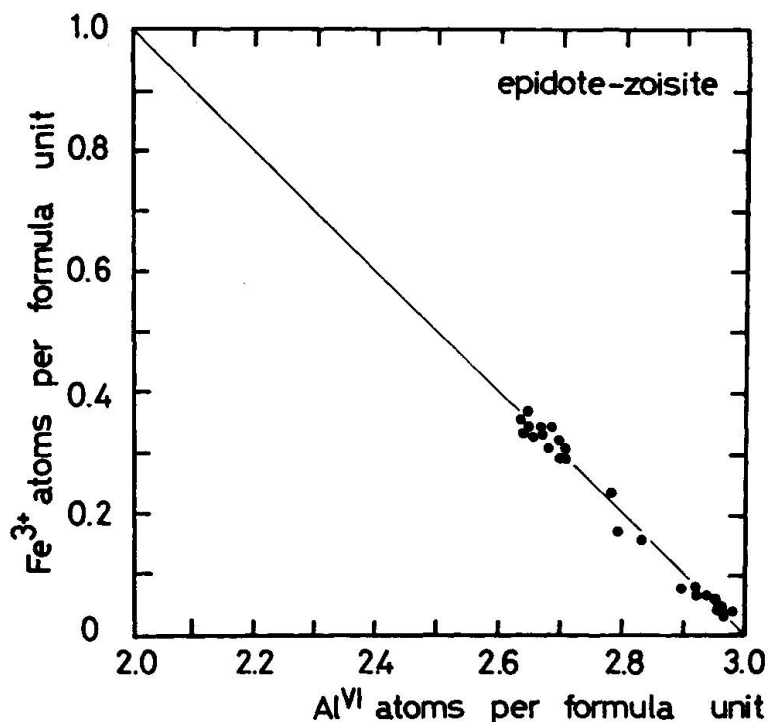


Fig. 21 Proportions of octahedral aluminum and ferric iron in epidote-zoisite group minerals.

higher-grade samples, chemical compositions tend to lie close to the zoisite end-member.

At one locality in the Steinental, Mn-rich epidote (pimontite) has been detected in quartzitic rock samples (meta-radiolarites?) coexisting with Mn-rich minerals such as Mn-garnet ( $\text{Spess}_{75}\text{Gross}_{14}\text{Pyr}_6\text{Alm}_5$ ), braunite and cryptomelan. Chemical analyses reveal variable Mn-contents in pimontite giving the following structural formula  $\text{Ca}_{1.6-1.9}\text{Mn}_{0.3-1.2}\text{Fe}_{0.3-0.7}\text{Al}_{1.8-2.0}\text{Si}_3\text{O}_{12}(\text{OH})$ .

#### PLAGIOCLASE

Detailed microprobe analyses were performed on 11 selected samples. The results are illustrated in Fig. 22 comparing the regional distribution of the samples with the frequency distribution of anorthite content observed within each sample. The results can be summarized as follows:

- In low-grade samples the anorthite content range from 17 to 33 mole percent. Within single grains local variations are in the order of 10 mole percent An.
- With increasing metamorphic grade the anorthite content increases continuously from 35 up to 90 mole percent (samples EF 41 to EF 806). At the same time a strong increase in the amount of modal plagioclase is observed.

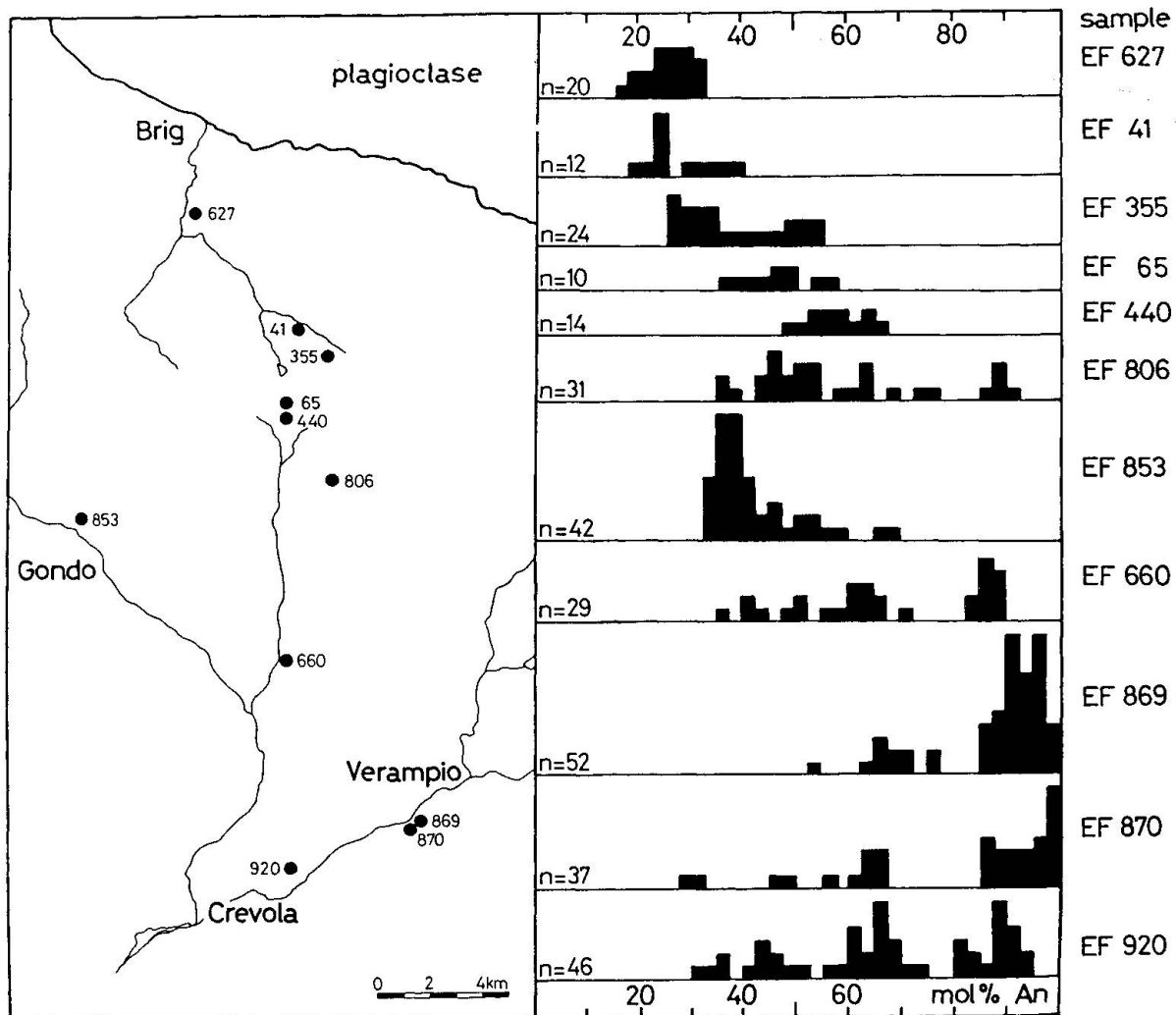


Fig. 22 Frequency distribution of plagioclase composition along the metamorphic profile Brig-Crevola.

- In the higher-grade samples, large compositional variations in An-content are found over small distances (10–200  $\mu\text{m}$ ), the An-content ranges from 30 up to 95 mole percent within one sample. Plagioclase are typically poikiloblastic and patchy zoned. Very often streaky, locally zoned domains reflect the shape of previously resorbed minerals such as white mica.
- Samples with low modal calcite tend to show smaller variations in anorthite content (sample EF 853).
- With exception of the peristerite gap, no other systematic miscibility gaps could be detected. The strongly zoned character of these plagioclases may be the result of very fine intergrowths of two different plagioclases in a submicron scale which cannot be resolved by conventional electron beam analyses (spot size of about 4  $\mu\text{m}$ ).

- Plagioclase coexisting with margarite-calcite-quartz becomes systematically enriched in anorthite with increasing grade, ranging from An<sub>30</sub> (samples from Brig) up to An<sub>58</sub> (samples from the Steinental area). FREY + ORVILLE (1974) and BUCHER et al. (1983) could show by graphical analysis of the subsystem CaO-Al<sub>2</sub>O<sub>3</sub>-SiO<sub>2</sub>-C-O-H that this compositional behaviour of plagioclase is mainly a function of metamorphic temperature.

#### K-FELDSPAR

Microprobe data indicate the presence of 6–12 mole percent albite (Fig. 23) and a very low anorthite content (0.1–1.1 mole percent). The rather high albite contents in k-feldspar result from the breakdown of muscovites having  $X_{Pa} = 0.12$ . Triclinity values, as defined by GOLDSMITH + LAVES (1954), were measured in three samples by Guinier-camera technique giving low values of 0.0–0.3

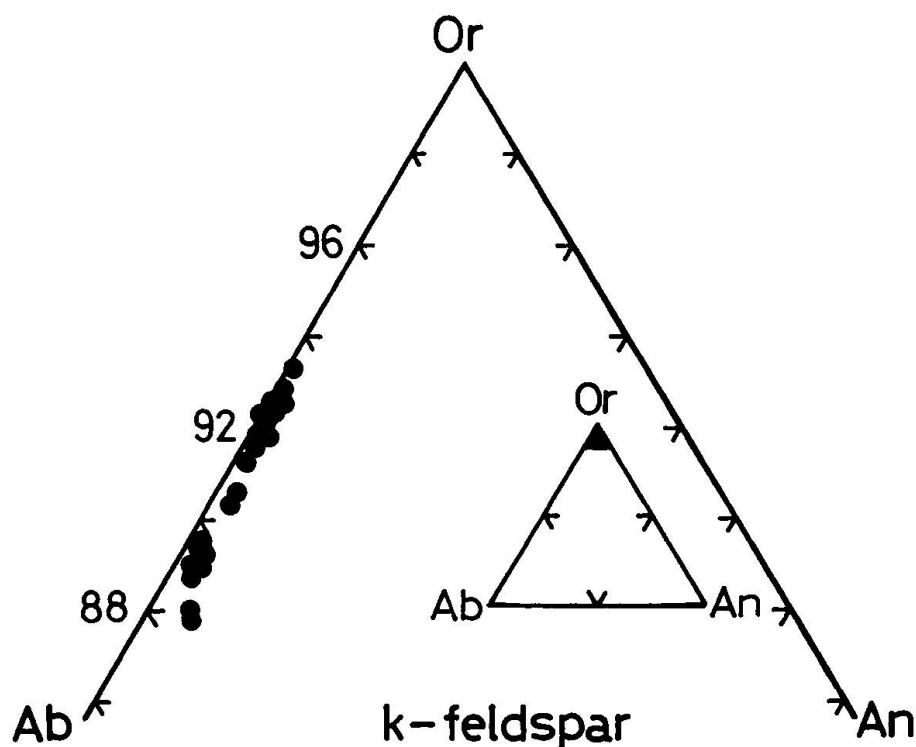


Fig. 23 Composition of K-feldspar in terms of Or-Ab-An components.

#### SCAPOLITE

Scapolite analyses have been calculated on the basis of 12 (Si+Al) (SHAW 1960). All the grains analyzed are more or less homogenous showing mizzonitic

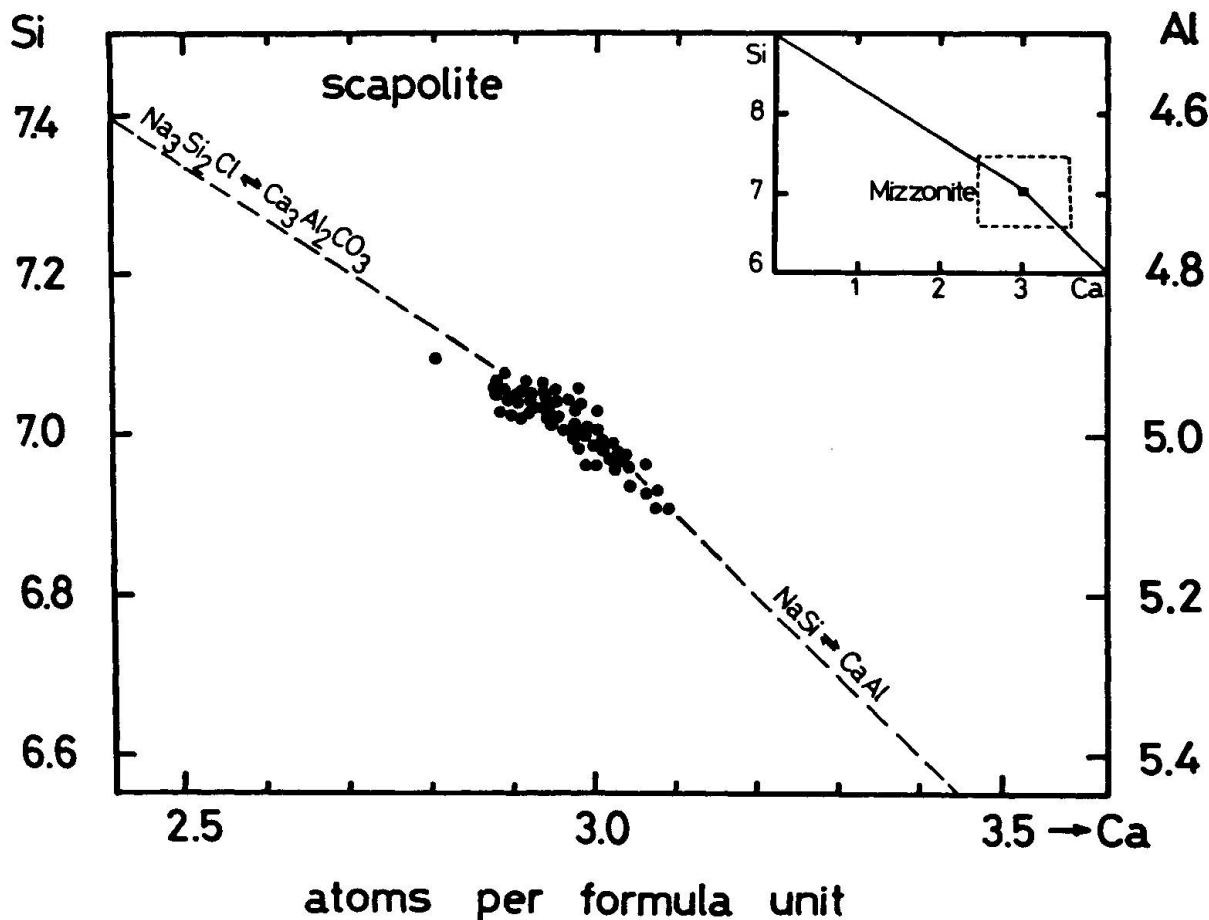


Fig. 24 Si-Ca variation diagram of scapolite. Analyses are calculated on the basis of  $12(\text{Si} + \text{Al})$  per formula unit of scapolite.

compositions corresponding to 74–79 percent meionite (Fig. 24). In terms of equivalent anorthite content (ELLIS 1978) the scapolites correspond to 64–70 percent EqAn. In all samples Cl and  $\text{SO}_4$  contents are very low (less than 0.15 wt. %).

#### STAUROLITE

The occurrence of staurolite is restricted to the pelitic layers. A limited number of microprobe analyses reveal only small chemical zonation with  $\text{Mg}/\text{Mg} + \text{Fe}$  increasing from core to rim. Minor amounts of Ti are present ranging up to 0.16 Ti per formula unit (Table 11). In some samples, substantial amounts of Zn can be observed (up to 2.4 wt. % ZnO) replacing mainly Fe. Within the same outcrop the Zn-content varies considerably depending upon modal staurolite content in the sample. This suggests that Zn is controlled mainly by local bulk composition and much less by metamorphic grade.

## CORUNDUM

Corundum was found in three samples occurring as very fine, prismatic or slightly rounded crystals which could optically be easily mistaken for zoisite. Chemical analyses show minor amounts of Si, Fe, Ti and traces of Cr (Table 12).

## GRAPHITE

Graphitic material was separated and analyzed by X-ray diffraction using the method described by GREW (1974). The crystallinity, defined as the peak-width at half peak height of the (002) basal reflexion indicates the presence of fully ordered graphite (LANDIS 1970). As a function of increasing metamorphic grade crystallinity values decrease from 0.5 for low-grade samples to 0.24 (2 $\theta$ ) for high-grade samples (Fig. 25).

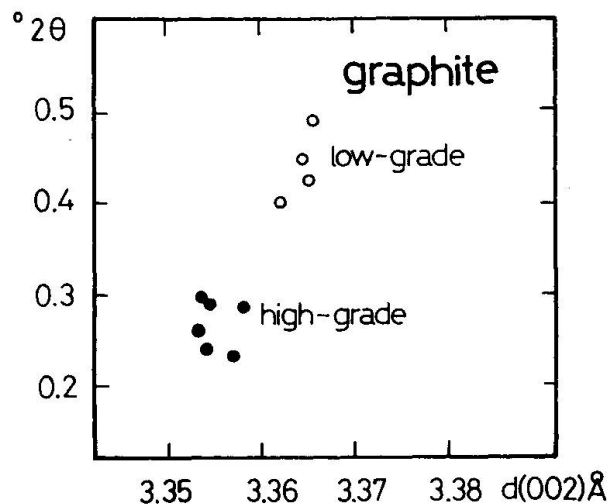


Fig. 25  $d(002)$  spacing values of graphite correlated to the crystallinity index defined as the peak width of  $d(002)$  at half peak height. Open circles: graphite from low-grade samples (Brig-Steinental). Filled circles: graphite from high-grade samples (Simplonpass).

## KYANITE

Representative analyses of kyanite show minor amounts of Fe (0.15–0.58 wt.%  $\text{Fe}_2\text{O}_3$ ). Ti and Cr are below the detection limit of the microprobe (less than 0.1 wt%).

## CARBONATE MINERALS

Calcite exhibits significant variation in composition, giving 1.2 to 4.2 mole percent  $\text{MgCO}_3$ , 1.4 to 4.5 mole percent  $\text{FeCO}_3$  and 0.2 to 2.0 mole percent  $\text{MnCO}_3$  (Fig. 26). Ferroan dolomite have been identified by staining method in only few samples.

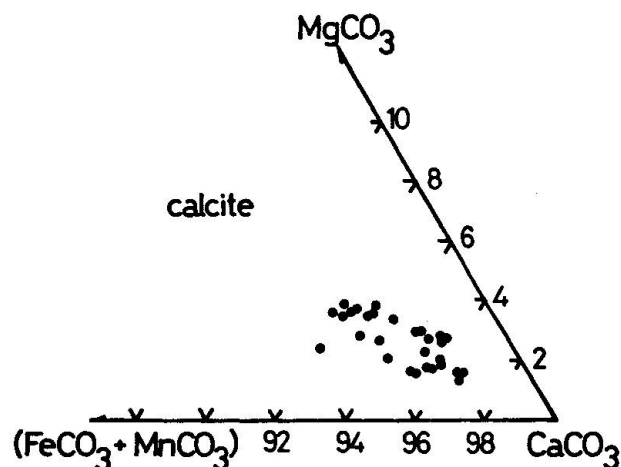


Fig. 26 Calcite composition in terms of  $\text{MgCO}_3$ - $\text{CaCO}_3$ - $(\text{FeCO}_3+\text{MnCO}_3)$  components.

## Metamorphic zonation

Based on the regional distribution of mineral assemblages analyzed in 320 samples different mineral zones and reaction-isograds could be identified and mapped along the cross-section which outline a gradual change in metamorphic grade from NW to SE. For the purpose of paragenetic analysis only *contacting mineral phases* have been considered to reflect mineral coexistence.

## MINERAL ZONE BOUNDARIES

Based on the first appearance criteria three mineral zone boundaries (Fig. 27) could be mapped in the northern part of the profile. These are the first appearance of biotite-calcite assemblages, the first appearance of almadine-rich garnet and finally the first appearance of tschermakitic amphibole. The reaction relations controlling the appearance of these phases could not be definitely deduced from the available data. Textural relations suggest the formation of biotite at the expense of both chlorite and muscovite as indicated by the preferential growth of first biotite along chlorite-muscovite rich layers (Fig. 28). This conclusion is supported by the substantial modal decrease of chlorite at

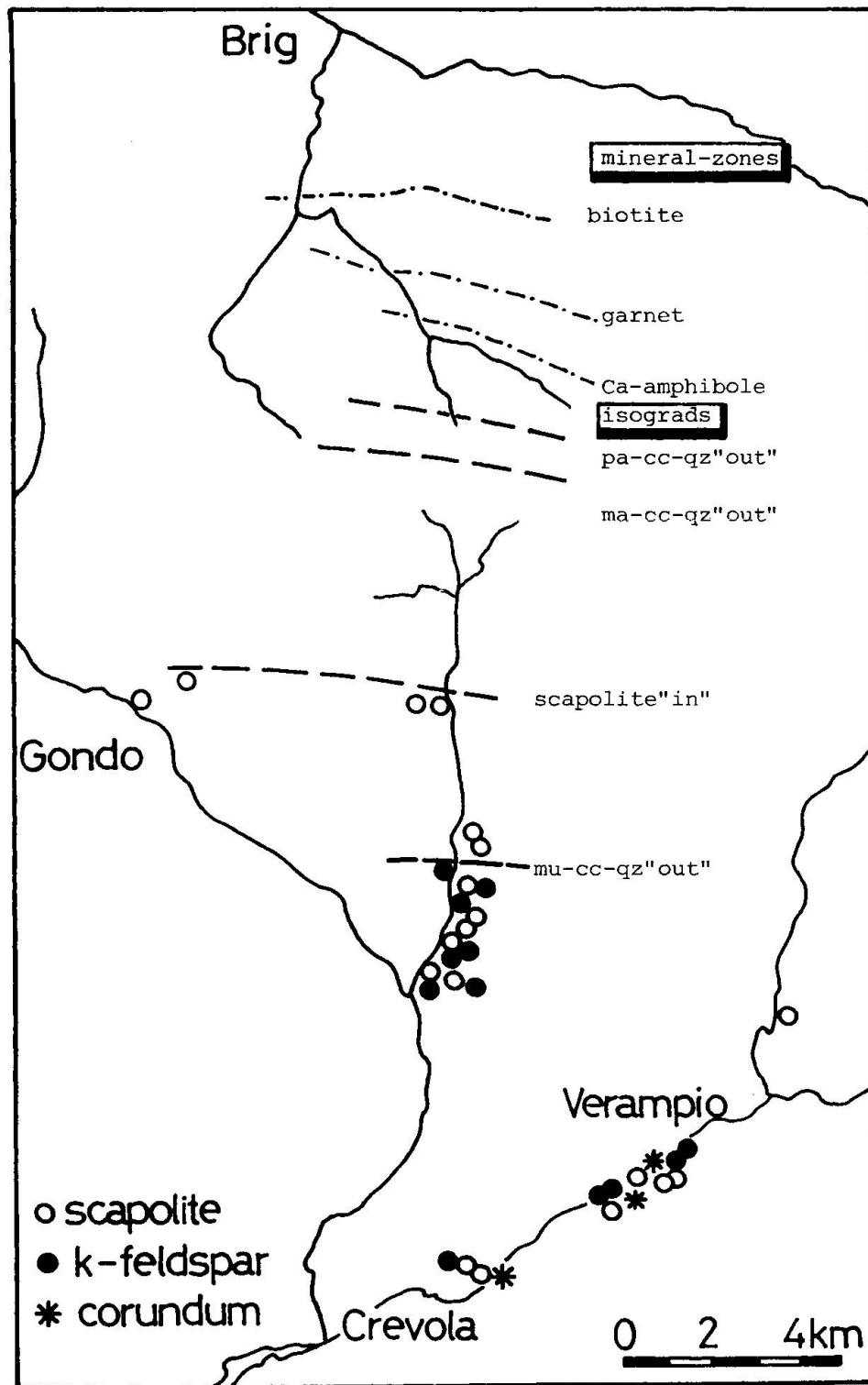


Fig. 27 Mineral zone boundaries and reaction isograds in calcareous rocks along the profile from Brig to Crevola.

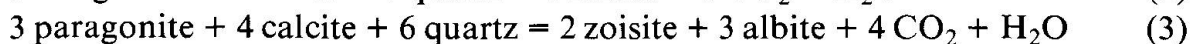
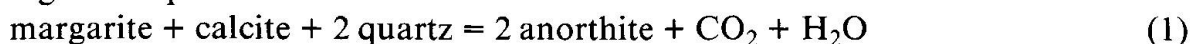
the expense of newly formed biotite as well as by the chemographic relations shown in Fig. 29. Chlorite, biotite and muscovite are chemically colinear with respect to Al-Fe-Mg suggesting the formal reaction chlorite + muscovite + quartz = biotite + H<sub>2</sub>O. No clear relations could be found controlling the first appearance of almandine-rich garnet. The systematic prograde chemical zoning of garnet, indicating complex Fe-Mn-Mg-Ca solid solutions as a function of metamorphic grade, suggests that the garnet forming reactions cannot be accounted for by a simple reaction. The first Ca-amphibole appears between mica and carbonate rich layers. The aluminous composition of these amphiboles implies that this mineral was formed by some reaction consuming Al-rich phases such as plagioclase (An-component) and white mica. The textural relations indicate that components from both the mica-rich and the carbonate-rich layers must have been involved in the reaction to form the Ca-amphibole. This implies mass-transport between these layers on a mm-scale. In some samples the amphiboles were replaced along their rims by biotite indicating extensive retrograde alkali-exchange with contacting muscovite.

#### ISOGRADS AND MINERAL REACTIONS

From the systematic changes of mineral assemblages and mineral modes as well as from compositional and textural relations found in thin sections the following mineral reactions were observed and mapped along the cross-section with increasing metamorphic grade (Fig. 27 and Fig. 30):

- paragonite-calcite-quartz "out" isograd
- margarite-calcite-quartz "out" isograd
- scapolite "in" isograd
- muscovite-calcite-quartz "out" isograd.

From the regional distribution pattern of two- and three-phase assemblages shown in figure 30 the stability relations of the white micas muscovite, margarite and paragonite relative to calcite-quartz can be studied. Paragonite and margarite coexisting with calcite-quartz are found to be restricted to the northern part of the cross-section. The upper stability of both assemblages can be mapped in the Simplonpass area defining the pa-cc-qz "out" and the ma-cc-qz "out" isograds. The following reactions limit the assemblage towards higher temperatures



Textural relations as well as the observed mineral modes suggest that the assemblage ma-cc-qz became unstable by reaction (1) rather than (2). The breakdown of margarite according to (1) has been seen in some samples containing

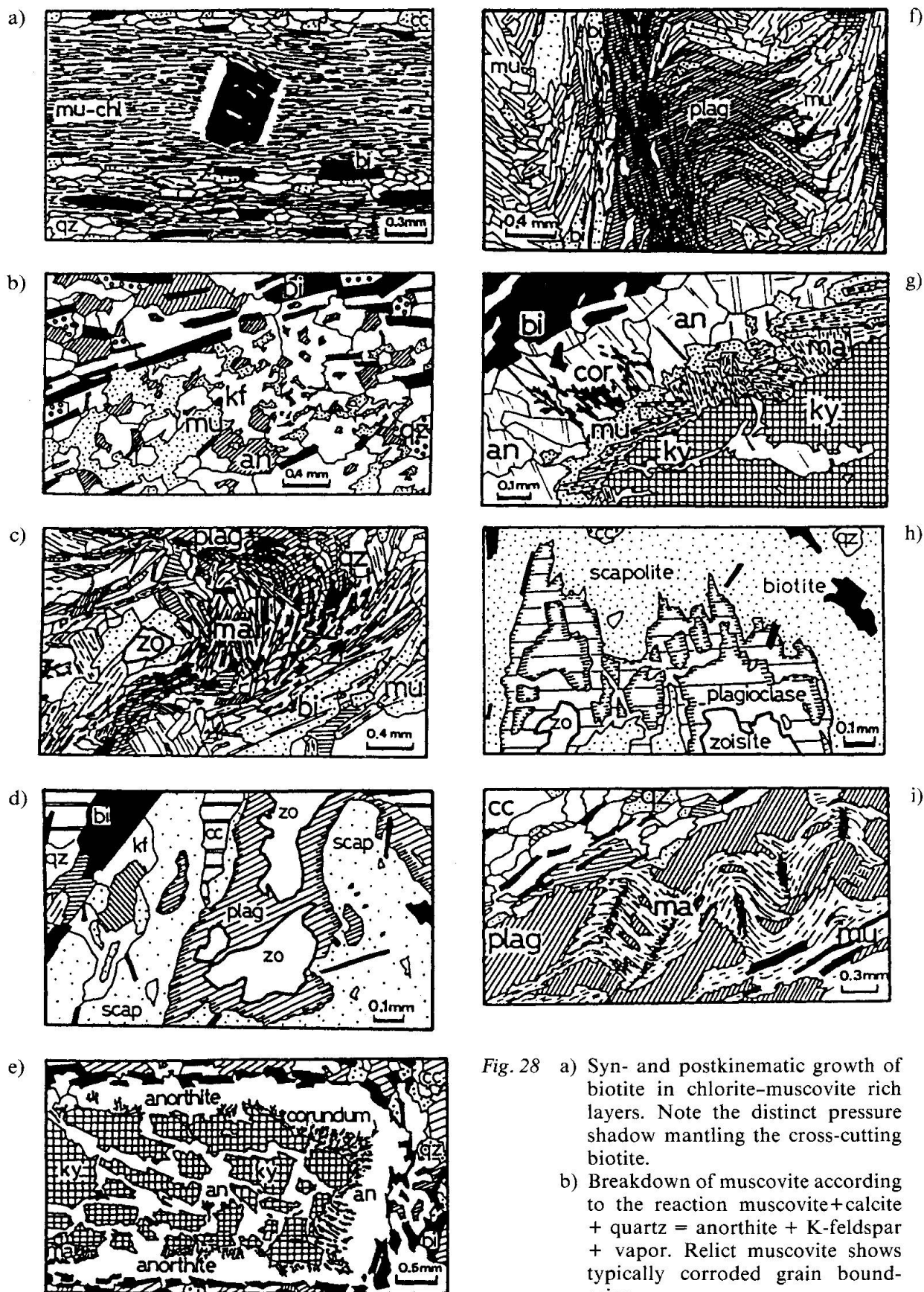


Fig. 28 a) Syn- and postkinematic growth of biotite in chlorite-muscovite rich layers. Note the distinct pressure shadow mantling the cross-cutting biotite.

b) Breakdown of muscovite according to the reaction muscovite + calcite + quartz = anorthite + K-feldspar + vapor. Relict muscovite shows typically corroded grain boundaries.

clear reaction textures of margarite being replaced by anorthitic plagioclase  $An_{50-65}$  (Fig. 28i). Margarite, previously in contact with calcite, is now found isolated from calcite and surrounded by plagioclase. In the calcite absent assemblages of the same area, margarite may have been newly formed postkinematically in coexistence with quartz and plagioclase (Fig. 28c).

If calcite is absent, paragonite-quartz and margarite-quartz remain stable to higher grade further to the south into the staurolite zone. In the two high-grade samples close to Verampio-Crevola, margarite was observed in the quartz-absent assemblages anorthite-margarite and kyanite-anorthite-margarite. Obviously metamorphic conditions must have exceeded the stability limits of the assemblage margarite + quartz.

Muscovite coexisting with calcite-quartz shows an increased stability range and remains stable up to the higher staurolite zone (Fig. 30). At higher grade within a short distance of some ten meters the breakdown according to the reaction



can be observed and mapped in the Cairasca valley. Textural relations between contacting mineral phases typically reflect this breakdown of muscovite as shown in Figure 28b. In local domains clear textural relations can be related to reaction (4) where one of the reactant phases (quartz or calcite) has been exhausted. Corroded muscovite is found in contact to K-feldspar ( $Or_{92}Ab_8$ ), plagioclase ( $An_{90}Ab_{10}$ ) and  $\pm$  quartz. Obviously calcite has been used up in this domain giving this "frozen-in" reaction texture. Note that biotite is not involved into this reaction. Furthermore replacement textures of muscovite by anorthitic plagioclase are quite common in the high-grade samples (Fig. 28f).

- 
- Fig. 28
- c) Postkinematic growth of margarite in the centre of a fold hinge traced by graphite.
  - d) Textural relations between calcite, scapolite, plagioclase, K-feldspar and zoisite. Zoisite does not appear in mutual contact to calcite any more, being strictly separated by anorthitic plagioclase.
  - e) Pseudomorphic replacement of coarse kyanite by anorthite and corundum. Obviously calcite was totally consumed by the reaction leading to this "frozen-in" reaction texture. Note the continuous border of biotite mantling this reaction texture. Corundum typically grows in fine crystals with some preferential radial orientation.
  - f) Postkinematic plagioclase helicically overgrowing mica-rich folds.
  - g) Detailed sketch map of the reaction zone showing corroded kyanite overgrown by random oriented coarse margarite plates. Some margarites are mantled themselves by muscovite suggesting extensive ionic exchange reactions involving a  $K^+$  rich vapor phase. On the left side is the reaction front consisting of anorthite and corundum.
  - h) Disequilibrium texture of a coexisting scapolite-plagioclase assemblage. Plagioclase contacting scapolite shows a strong gradient in anorthite content, decreasing from  $An_{92}$  close to zoisite to  $An_{61}$  when contacting scapolite.
  - i) Reaction texture showing the replacement of margarite, calcite and quartz by plagioclase.

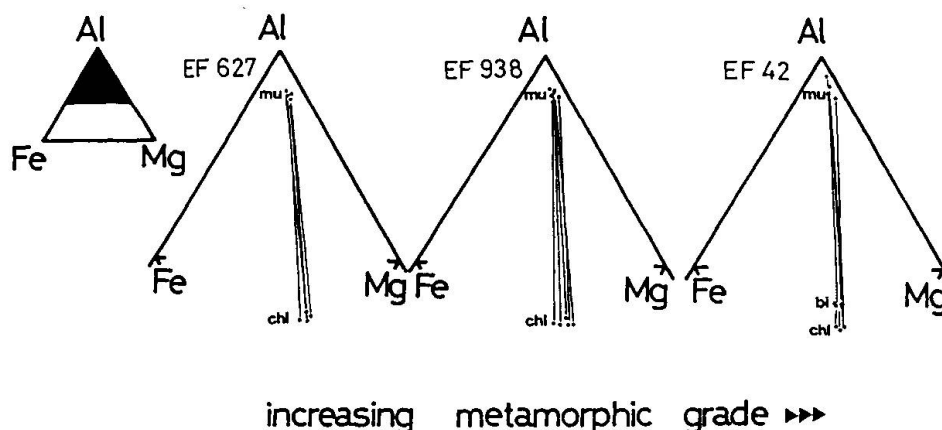


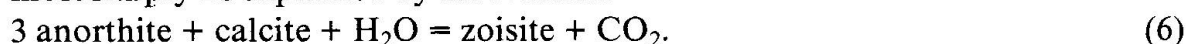
Fig. 29 Partitioning of Al-Fe-Mg between coexisting chlorite, muscovite and biotite across the biotite mineral zone boundary.

The scapolite-“in” isograd can be related to the continuous reaction

$$3 \text{ anorthite} + \text{calcite} = \text{meionite} \quad (5)$$

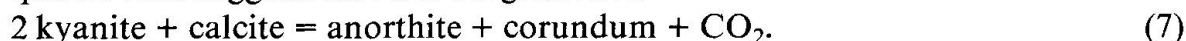
First meionitic scapolite (75 mole percent meionite) was observed in calcite-plagioclase assemblages replacing these phases. This suggests a higher thermal stability of meionite-calcite relative to plagioclase-calcite when the plagioclase was more basic than  $\text{An}_{60-68}$ . This limit defines the rather sharp boundary for the scapolite-“in” isograd (Fig. 27).

In the high-grade samples, zoisite is typically rimmed by anorthitic plagioclase separating zoisite from the matrix-calcite (Fig. 28d). These textures can most simply be explained by the reaction

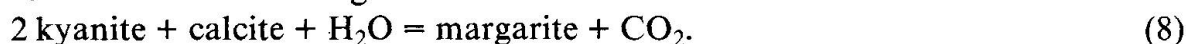


This reaction requires a net addition of  $\text{H}_2\text{O}$  rich fluids.

In a few samples near Verampio-Crevola the breakdown of kyanite to corundum and anorthite can be observed in calcareous specimens containing matrix minerals such as calcite, scapolite, plagioclase, K-feldspar, biotite and quartz. This suggests the following reaction



Anorthitic plagioclase ( $\text{An}_{98-100}$ ) typically grew pseudomorphic after kyanite, preserving the primary shape of the kyanite crystal. In some places where calcite was consumed, kyanite may be still present showing a reaction rim consisting of anorthite ( $\text{An}_{98-100}$ ) and corundum. This arrested reaction texture suggests that mineral equilibria was attained only in small local domains since a few hundreds of microns away calcite is still present in the matrix of the rock sample (Fig. 28e). In some places, coarse margarite plates have been observed coexisting with corroded kyanite (Fig. 28g). This margarite may have been formed either according to the reaction



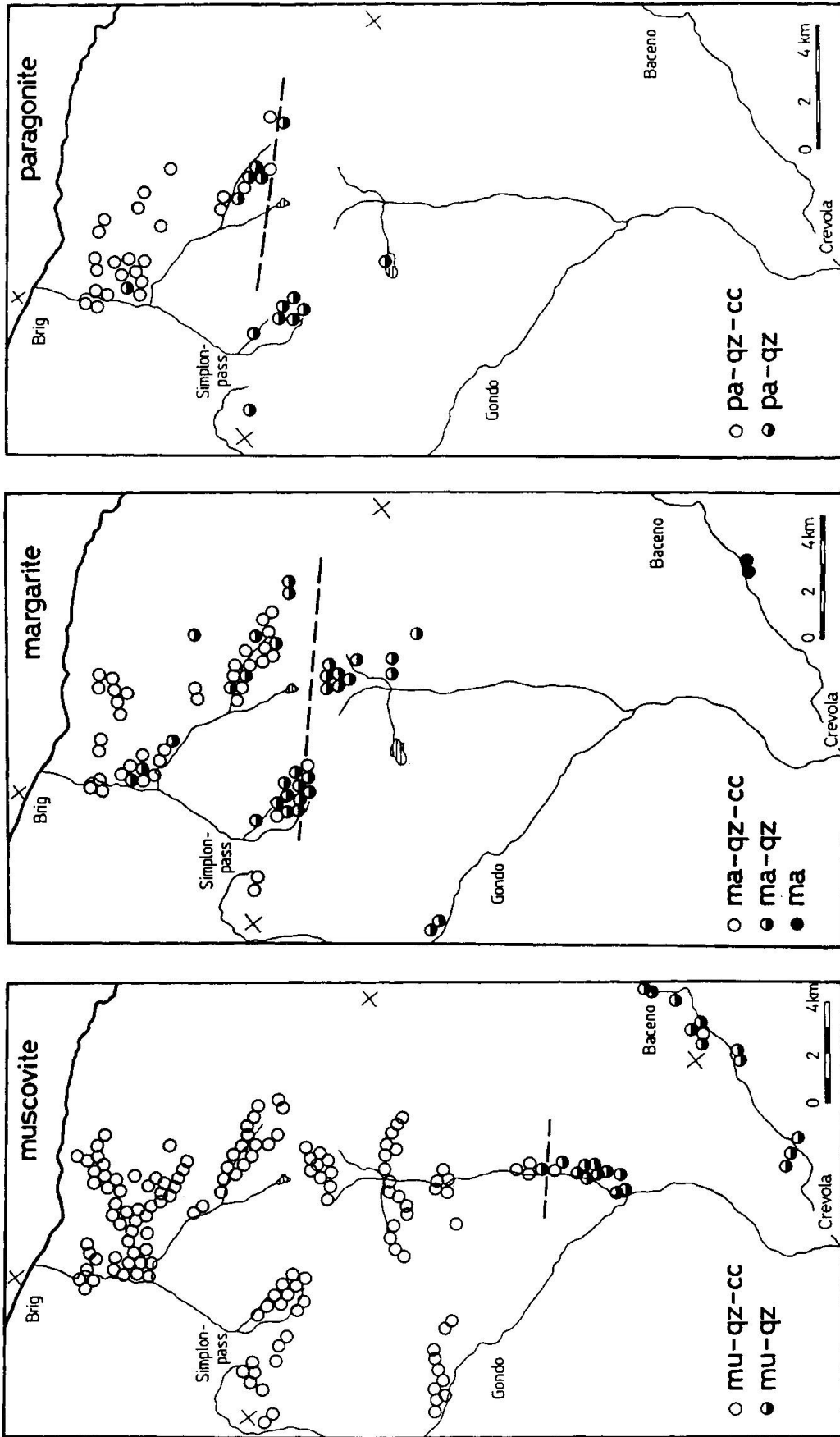


Fig. 30 Regional distribution pattern of two- and three-phase assemblages:

- muscovite-calcite-quartz, muscovite-quartz
- margarite-calcite-quartz, margarite-quartz
- paragonite-calcite-quartz, paragonite-quartz

or it may indicate a retrograde replacement of the assemblage anorthite–corundum by margarite. From the close textural relation to kyanite reaction (8) seems to be more likely.

Regarding the presence of corundum, it is interesting to note that quartz is present in the rock matrix only 80–140 microns away from corundum. Apparently there was no chemical communication between these two incompatible minerals such as if they existed in isolated bulks. Chemical equilibration must have been restricted to local domains (micron scale).

High-grade samples very often reveal crystals of rutile which are overgrown by sphene suggesting the following reaction



### Estimate of metamorphic P-T conditions

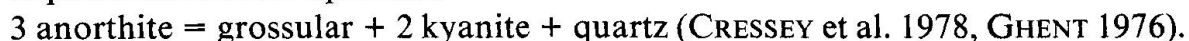
P-T conditions of metamorphism can be estimated by utilizing calibrated geothermometers and barometers, by comparing the stability relations of observed mineral assemblages with experimental data and by considering quantitative thermodynamic calculations.

### PRESSURE

The estimation of pressure is rather difficult because the critical mineral assemblages are quite rare. In the low-grade samples (Brig) typical pressure-dependent mineral equilibria are absent. In the medium and higher-grade samples two estimates can be made based on the presence of kyanite and on the Ca partitioning between coexisting garnet–plagioclase mineral pairs in the assemblage garnet–plagioclase–kyanite–quartz.

In all high-grade samples kyanite is the widespread  $\text{Al}_2\text{SiO}_5$  phase coexisting with garnet and/or staurolite. Assuming that these high-temperature minerals equilibrated within the stability field of kyanite, which is supported by textural evidence, minimum pressures of about 5–6 kb can be deduced considering the experimental data of the alumosilicate triple point of RICHARDSON (1969) and HOLDAWAY (1971).

Metamorphic pressures can be furthermore estimated from the partitioning of Ca between coexisting garnet and plagioclase according to the pressure-dependent mineral equilibria



Since mineral compositions found in our rocks are not pure endmembers, terms for activity for the anorthite component in plagioclase and the grossular component in garnet have to be estimated. For the present calculations the ap-

proximation proposed by GHENT (1979) has been used which includes an empirical estimate of the activity coefficient product ( $K\gamma$ ). According to GHENT (1979) this geobarometer has a resolution of about  $\pm 1.6$  kb (two standard deviations). The pressure estimates listed in table 14 indicate consistently high pressures of 6 to 7.8 kb for all samples along the southern part of the cross-section (Simplonpass-Crevola).

## TEMPERATURE

### Fe-Mg cation exchange thermometry (garnet-biotite)

Temperatures can be calculated from the Fe-Mg partitioning between coexisting garnet-biotite mineral pairs. The temperature dependence of the distribution coefficient  $K_D$  (Mg-Fe) has been previously calibrated empirically by GOLDMANN + ALBEE (1977) and THOMPSON (1976) as well as experimentally by FERRY + SPEAR (1978). In the lower temperature range (450–600 °C) the calibrations are consistent with each other while at higher temperatures some significant deviations are observed. For the present study the calibration of FERRY + SPEAR is used.

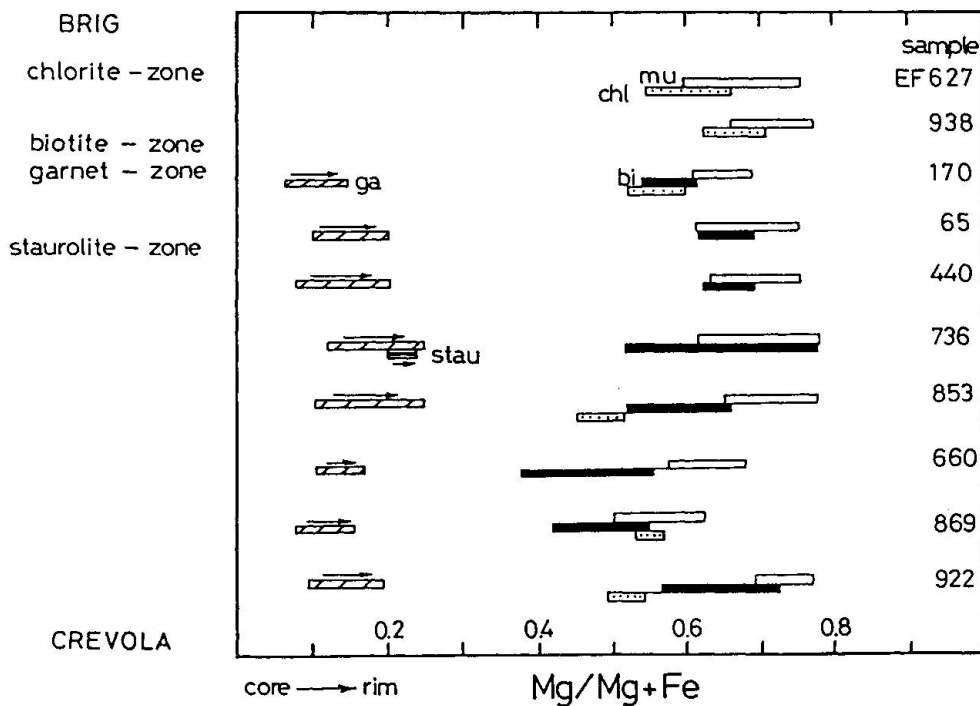


Fig. 31 Variation and change of Mg/Mg+Fe in garnet, staurolite, biotite, chlorite and muscovite along the cross section Brig-Crevola.

In our samples a regular preference of Mg relative to Fe can be observed for the most important Fe-Mg-minerals with  $Mg/Mg+Fe$  ratios increasing in the order garnet < staurolite < chlorite, biotite < muscovite (Fig. 31). In most minerals, a rather wide spread in  $Mg/Mg+Fe$  can be found on the scale of cm to mm within a thin section or even within one single mineral grain (garnet). All garnets consistently show strong compositional zoning reflecting prograde modification from core to rim with increasing  $Mg/Mg+Fe$  ratios. The largest variations in  $Mg/Mg+Fe$  ratios can be observed for biotites which exhibit distinctly different ratios depending upon their textural relations with other minerals. Biotites coexisting with garnets are enriched in Fe relative to isolated biotites in the rock matrix. This observation can be related to the exchange reaction for iron and magnesium between biotite and garnet which is mainly controlled by temperature (THOMPSON 1976). As a function of increasing temperature the two-phase exchange tends to decrease the difference in  $Mg/Mg+Fe$  between these two minerals. This relation is shown in Fig. 32 for sample EF 736 docu-

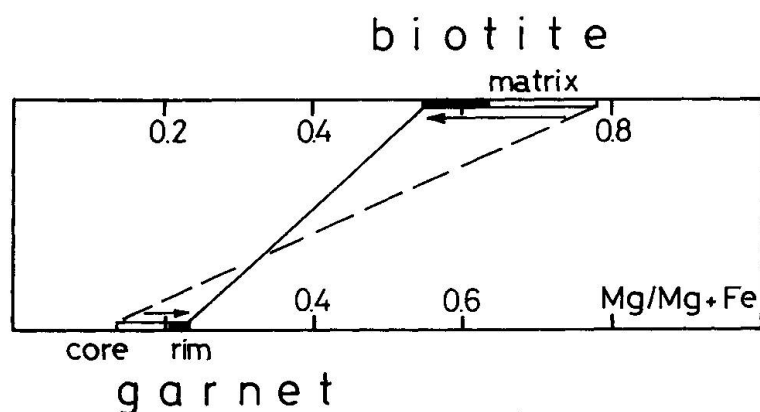


Fig. 32 Mg-Fe partitioning between coexisting garnet and biotite (EF 736) indicating the shift of tie-lines with progression of metamorphism (further explanations in the text).

menting the prograde evolution of biotite and garnet with respect to  $Mg/Mg+Fe$ . From this reaction scheme we may conclude that isolated biotite in the rock matrix and garnet-core compositions still reflect their initial  $Mg/Mg+Fe$  ratios from equilibration at some lower temperature ("refractory" behaviour). Obviously prograde Fe-Mg exchange occurred only on a very local scale between contacting mineral grains. Because of these problems with the range for equilibrations all temperatures deduced here were measured on adjacent garnet rim-biotite mineral pairs (table 15). The results are illustrated in Fig. 33 comparing the regional distribution of the samples with their corresponding  $K_D$ -values. For comparison, the calibration for 400, 500 and 600 °C according to FERRY + SPEAR is shown on the diagram. In all samples a systematic wide range of  $K_D$  can be found although a general trend of the temperature-estimates is obvious.

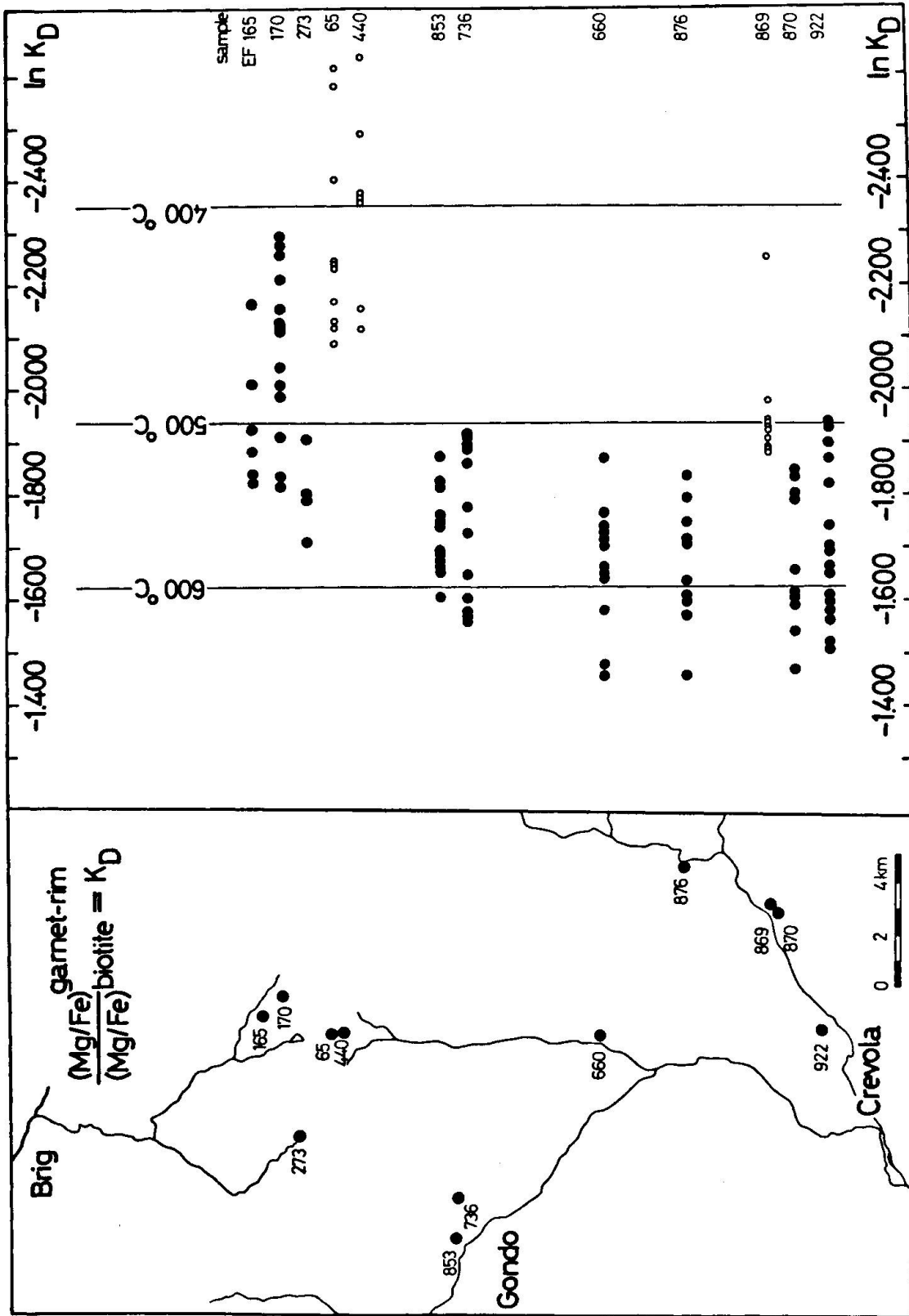


Fig. 33 Regional variation of biotite-garnet  $\ln K_D$  (Mg-Fe) values along the cross section from Brig to Crevola.

The trend suggests temperatures around 450–540 °C in the northern part and 520–630 °C in the southern part. The estimated analytical error in temperature is about  $\pm 26$  °C (two standard deviations) based on a analytical error of 1.5% in MgO and FeO analyses. For some samples (EF 65,440 and 869), illustrated by open circles, very low temperatures are calculated which may reflect local retrograde Fe–Mg exchange during the later stages of the metamorphism. The scatter of temperature values within one single thin section (few mm to cm scale) indicates that either chemical equilibrium was not or only partially attained, or that some of the solid solutions may exhibit non-ideal behaviour or that there may be displaced equilibria caused by other elements such as Mn, Ca in garnet and Ti, Al in biotite. However, this latter effect can be excluded since within a single sample, garnet-rims and contacting biotites have rather constant compositions with respect to these elements mentioned above, revealing no systematic correlation to the  $K_D$  (Mg–Fe) values. Thus the wide spread in  $K_D$  values most probably reflects some incomplete, local attainment of chemical equilibria due to the strong compositional change of garnet and biotite during prograde metamorphism. Obviously cation exchange processes occurred on very local domains including only the portions of the minerals in direct contact to each other.

#### **Paragonite–kyanite–albite–quartz equilibria**

From quantitative calculations of the white mica-feldspar phase relations presented by THOMPSON (1974), the thermal stability of the four phase assemblage paragonite–kyanite–albite–quartz is restricted to a small temperature range of 520–530 °C. This assemblage was observed in carbonate-free rocks in the Simplonpass area (paragonite-rich schists). Coexisting plagioclase in these rocks reveals oligoclase composition ( $An_{16-18}$ ), hence the activity coefficient for albite component in plagioclase is about unity. THOMPSON (1974) suggested that the stability field for these minerals was only slightly sensitive to pressure.

#### **Talc–tremolite–calcite–dolomite–quartz equilibria**

According to the experimental data presented by SLAUGHTER et al. 1975 the isobaric, invariant, five-phase assemblage talc–tremolite–calcite–dolomite–quartz observable in the Steinental suggests minimum temperatures of about 450–480 °C if pressures of 2–5 kb are assumed. Microprobe analyses on sample EF 137 reveals no fluorine present in tremolite, however substantial amounts of aluminium are found (up to 6.0 weight percent  $Al_2O_3$ ) which increases the stability range of tremolite and depresses the temperature for the invariant assemblage talc–tremolite–dolomite–calcite–quartz.

### Muscovite–paragonite thermometry

Temperatures measured for the muscovite–paragonite solvus by EUGSTER + YODER (1972) give unrealistic high temperatures of  $> 600\text{ }^{\circ}\text{C}$ , a problem that has already been reported by FREY (1969) and FOX (1975). However, using the correlation between muscovite–paragonite and calcite–dolomite, as proposed by ROSENFELD (1969), more reasonable temperatures of about  $420\text{ }^{\circ}\text{C}$  at Brig increasing to  $500\text{--}540\text{ }^{\circ}\text{C}$  at the Simplonpass can be calculated.

### Scapolite–calcite–plagioclase thermometry

According to experimental studies (GOLDSMITH + NEWTON 1977) the partitioning of Ca and Na between coexisting scapolite–plagioclase is strongly temperature dependent making it a potential geothermometer. In our high-grade samples, the three-phase assemblage scapolite–plagioclase–calcite is very common allowing the use of this thermometer. In Fig. 34 tie-lines of coexisting scapolite–plagioclase (contacting mineral pairs) are plotted, while Fig. 35 shows the corresponding sample locations and the observed phase relations. At a distinct equilibration temperature, the Na–Ca distribution between contacting plagioclase and scapolite should be fixed by the three-phase assemblage scapolite–plagioclase–calcite according to reaction (5). However, plagioclases in contact with scapolite show large variations in anorthite content while the Ca/Ca+Na ratio of scapolite remains rather constant. This may suggest that either equilibrium was not attained or scapolite and plagioclase show some non-ideality in their solid solution or there may be some ordering effects or there are some retrograde mineral reactions. The textural and compositional relations illustrated in Fig. 28h show that disequilibrium may be important in the three-phase assemblage scapolite–plagioclase–calcite suggesting that calcite is not involved anymore in reaction (5). This implies that thermal equilibration is restricted to contacting scapolite–plagioclase grainboundaries. Using the scapolite–calcite–plagioclase temperatures as calibrated by GOLDSMITH + NEWTON (1977) the samples has calculated temperatures that are too high ( $> 750\text{ }^{\circ}\text{C}$ ). Recently the scapolite geothermometer was recalibrated by OTERDOOM (1979). He compared the stability relations of scapolite in argillaceous rocks at the west border of the Bergell with temperatures deduced independently from garnet–plagioclase–wollastonite–quartz and calcite–amphibole–diopside–quartz assemblages in this area. His results show that the first scapolite (66–70 EqAn) coexisting with anorthitic plagioclase and calcite appears at temperatures of about  $530\text{--}550\text{ }^{\circ}\text{C}$  which is in close agreement to our results. First scapolite of 65–69 EqAn can be observed within the staurolite zone in the Cairasca-valley where temperatures of  $> 550\text{ }^{\circ}\text{C}$  have been calculated by other means.

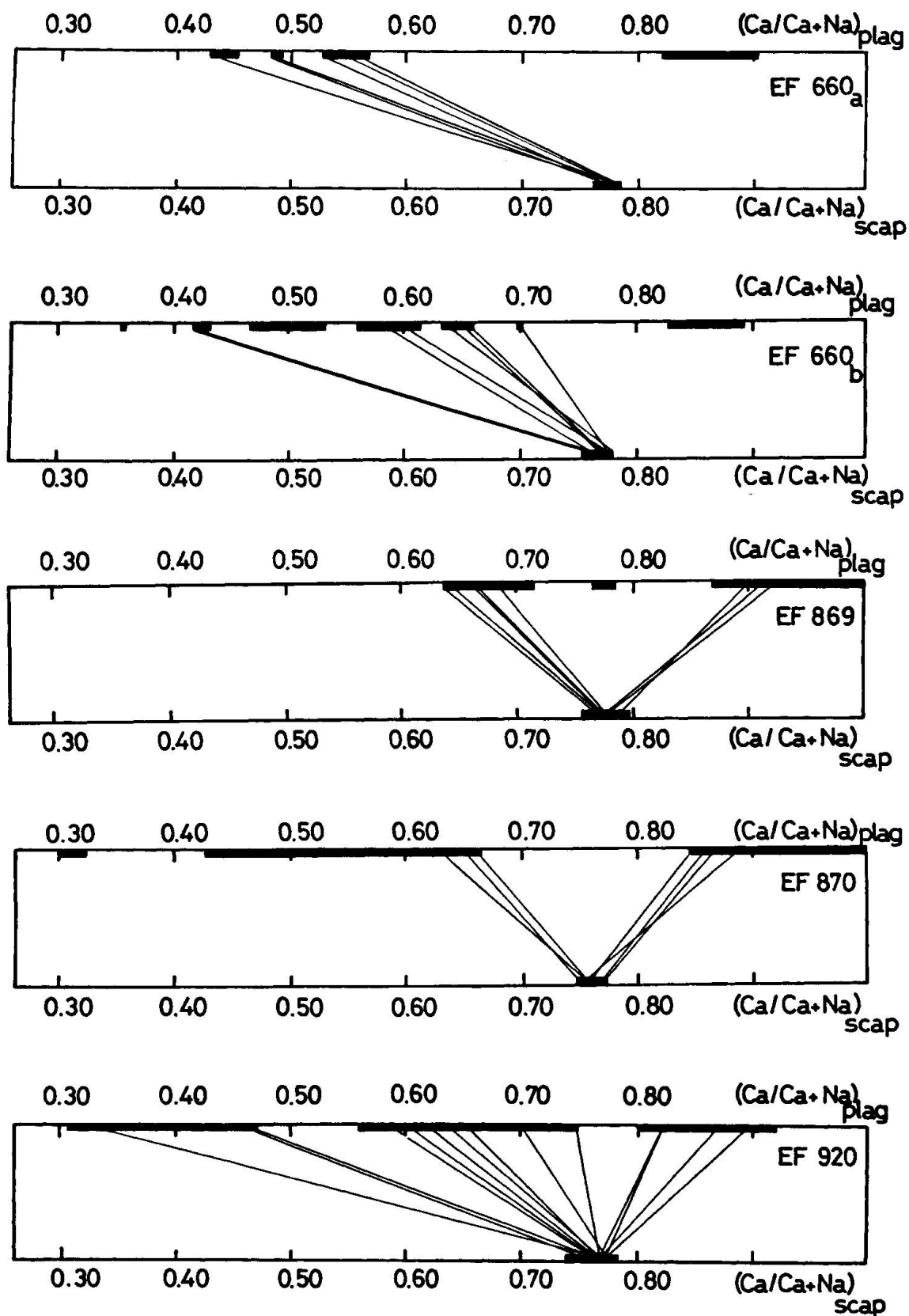


Fig. 34 Tie-lines of coexisting plagioclase–scapolite in rock samples containing excess calcite.

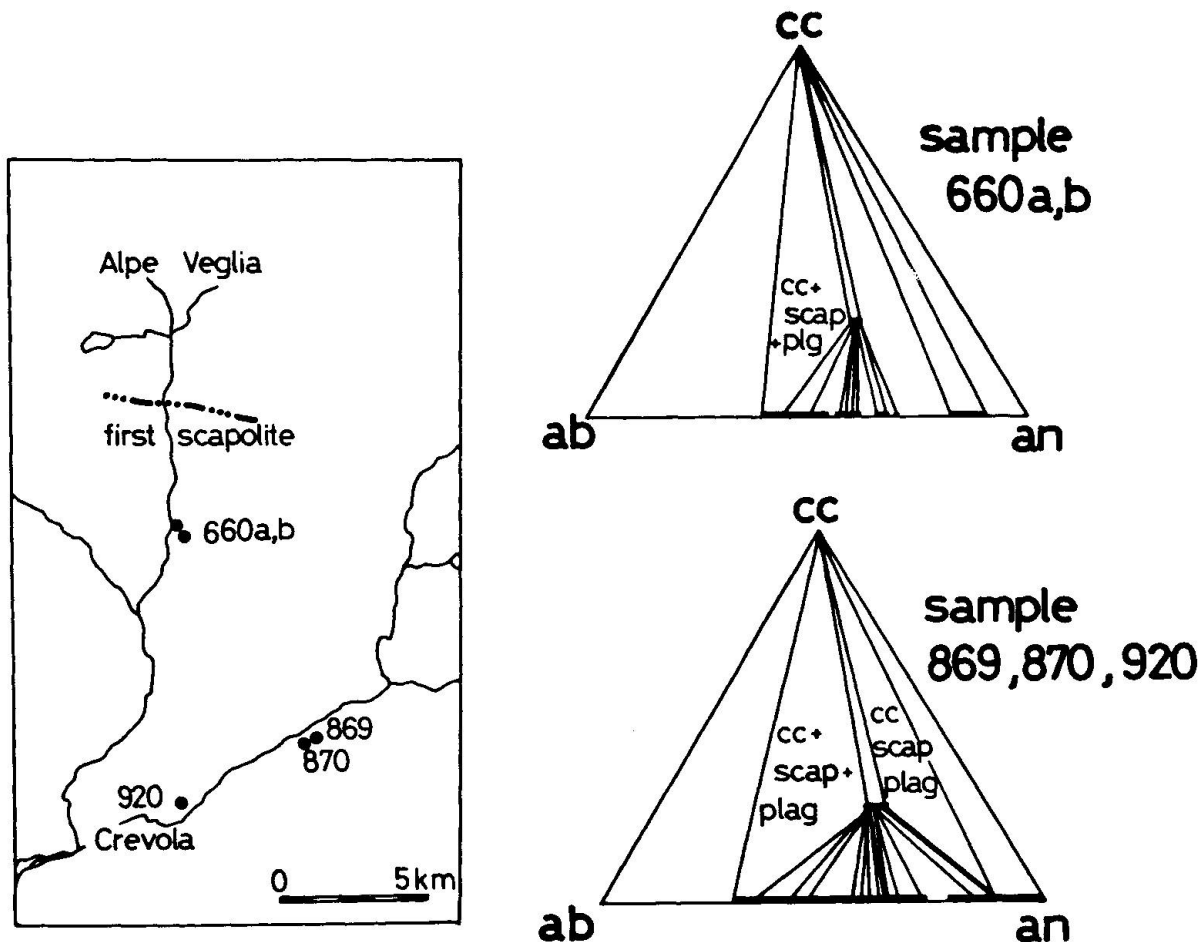


Fig. 35 Chemographic relations of scapolite-plagioclase-calcite assemblages.

#### Upper stability of margarite

From the margarite stability relations as described by CHATTERJEE (1976) and BUCHER et al. (1983) margarite-bearing assemblages have a quite restricted stability range giving some temperature limits. CHATTERJEE (1976) showed that the assemblage margarite-staurolite-quartz has a very limited stability field from 540 to 560 °C at 6 to 7 kb. Generally the assemblage margarite-quartz remains stable up to 500–560 °C for  $P_{H_2O}$  of 4 to 8 kb. This temperature will be lowered if  $CO_2$  is present in addition in the fluid phase by about 15 °C for a decrease in  $a_{H_2O}$  of 0.1. However, this effect is countered by the incorporation of some paragonite component into margarite (CHATTERJEE 1976). Thermodynamic calculations of the equilibria margarite + calcite + quartz = anorthite + vapor indicate temperatures of about 490–520 °C at 4–6 kb for the margarite-calcite-quartz “out” isograd in the Simplonpass area (BUCHER et al. 1983). Along our cross-section Brig-Crevola, the assemblage margarite-plagioclase reveals a sys-

tematic change in composition, showing increasing Ca/Ca+Na ratios for both minerals with increasing grade, ranging up to margarite ( $\text{Ma}_{92}\text{Pa}_8$ ) and plagioclase ( $\text{An}_{100}$ ). This compositional behaviour is mainly controlled by metamorphic temperature (BUCHER et al. 1983). From graphical analysis of the system  $\text{CaO-Na}_2\text{O-Al}_2\text{O}_3\text{-SiO}_2\text{-H}_2\text{O-CO}_2$  presented by FREY + ORVILLE (1974) the assemblage paragonite-calcite-quartz has some lower stability compared to margarite-calcite-quartz which is consistent to our field data (Fig. 30).

The occurrence of the assemblages margarite-anorthite and margarite-kyanite-anorthite in sample EF 870 indicates that the upper stability limit of margarite defined by the reaction margarite = anorthite + corundum +  $\text{H}_2\text{O}$  has not been exceeded (Fig. 36) which limits maximum temperatures to less than  $620^\circ\text{C}$  at 6 kb (CHATTERJEE 1976).

#### Upper stability of muscovite + calcite + quartz

The breakdown of muscovite + calcite + quartz according to reaction (4) can be used to obtain the minimum temperature for the rocks under consideration. The equilibrium temperature for this reaction has been determined experimentally by HEWITT (1973) giving temperatures of  $570\text{--}600^\circ\text{C}$  at 6–7 kb, assuming  $x_{\text{CO}_2} = 0.3$ .

#### Upper stability of kyanite + calcite

Using the thermodynamic data of HELGESON et al. (1978) equilibrium temperatures can be calculated for the observed mineral reaction 2 kyanite + calcite = anorthite + corundum +  $\text{CO}_2$  (7). At 6–7 kb and  $x_{\text{CO}_2} = 0.3$  the equilibrium temperatures are in the order of  $550\text{--}580^\circ\text{C}$ .

#### Graphite-geothermometer

Some estimates on metamorphic temperature conditions can be deduced from the crystallinity of graphitic material in the samples (GREW 1974, LANDIS 1970, SHENGELIA et al. 1977). The crystallinity of graphite is mainly controlled by temperature, the influence of pressure is only of minor importance. Since graphite is not sensitive to retrograde alteration, the crystallinity reflects the highest temperature condition reached in a rock sample. The crystallinity values observed in our samples (Fig. 25) point to higher amphibolite facies conditions for the samples from the Simplonpass area which is compatible with temperatures of  $550\text{--}600^\circ\text{C}$  (GREW 1974).

### Fluid composition

The presence of hydrous phases, carbonates and graphite indicates a C-H-O fluid. From the study of FRENCH (1966) and EUGSTER + SKIPPEN (1967) metamorphic fluids coexisting with graphite are dominantly rich in H<sub>2</sub>O for metamorphic conditions as observed in our area. Furthermore, the presence of margarite and zoisite, as observed in many samples, restricts the fluid composition to rather low  $x_{\text{CO}_2}$  (NITSCH + STORRE 1972, CHATTERJEE 1976). Reaction textures suggest that fluid phases had been buffered along the reaction curves as long as all minerals involved into the reaction have been present.

### Conclusions

The metamorphic temperature gradient is well defined along the cross-section. A systematic increase in temperature from about 400 °C (Brig) up to 580–620 °C (Crevola) is observed (Fig. 36). Pressure estimates remain relatively uncertain for samples from the low-grade part of the cross-section. In this area, POTY et al. (1974) estimated minimum pressures of about 2.5–2.8 kb from calculated densities of fluid inclusions in Alpine fissure minerals.

In the higher-grade part (Simplonpass–Crevola) pressures of about 6–8 kb can be deduced.

Microprobe data as well as paragenetic relations show that chemical equilibration is restricted to local domains of contacting minerals (mosaic equilibrium textures). Domain size is found to vary according to the different elements, mineral species and grain sizes in the range of few microns to several hundreds of microns.

Combining the present P-T data with available isotopic mineral age data from this area provides some insight into the *temperature-pressure-time* relations of the Alpine orogeny. The different temperatures at which minerals become closed system with respect to retaining decay products allows to estimate the cooling and uplift rate in this area. From concordant U-Pb monazite ages KÖPPEL + GRÜNENFELDER suggested that high-temperature conditions prevailed until 30 to 20 my ago in the southern part of the cross-section (Crevola). Along the cross-section Brig–Crevola throughout uniform young Rb-Sr biotite and K-Ar muscovite retention ages of 8–13 my have been found (JAEGER et al. 1969, HUNZIKER et al. 1969 and FRANK 1979) dating the time when the rocks cooled below the critical blocking temperatures for radiogenic Sr and Ar respectively, corresponding to temperatures of about  $300 \pm 50$  °C (Fig. 37). The age pattern indicates a more or less horizontal cooling-isotherme (FRANK 1979) which crosscuts tectonic boundaries as well as metamorphic isograds. This implies a differential cooling and uplift regime along the cross-section, beginning

Fig. 36 Compilation of P-T estimates along the cross section Brig-Crevola (B = Brig, S = Steinental, SP = Simplonpass, C = Crevola). Some calibrated reactions relevant to this study are:

- 1) talc-tremolite-calcite-dolomite-quartz equilibria (SLAUGHTER et al. 1975)
- 2) margarite + calcite + quartz = anorthite + vapor (BUCHER et al. 1983)
- 3) muscovite + calcite + quartz = k-feldspar + anorthite + vapor (HEWITT 1973, a-c referring to  $x_{\text{CO}_2}$  = 0.3, 0.4 and 0.5)
- 4) margarite = anorthite + corundum +  $\text{H}_2\text{O}$  (CHATTERJEE 1974)
- 5) Al-silicate phase relations according to RICHARDSON et al. 1969
- 6) Al-silicate phase relations according to HOLDAWAY 1971

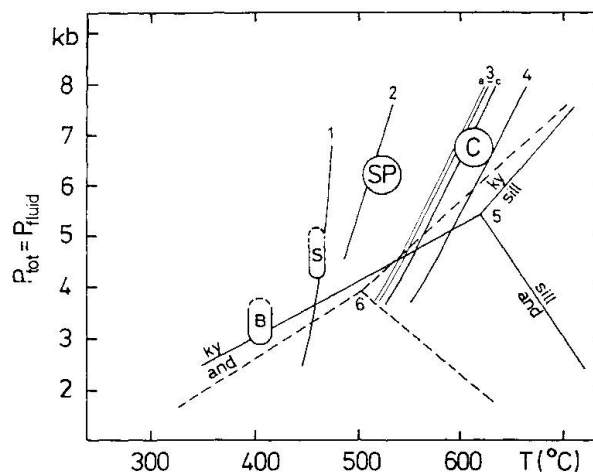
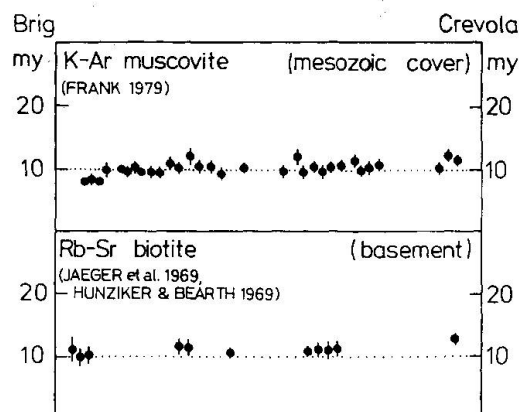


Fig. 37 Summary of apparent mineral ages in the profile between Brig and Crevola (mesozoic cover rocks and crystalline basement).



with much faster cooling-rates in the SE (Crevola) and a slower cooling in the NW at Brig. Therefore the steeply dipping isograd pattern observable today in this area (STRECKEISEN + WENK 1974 and this study) must be considered at least partially as the result of a postmetamorphic updoming of the deepest tectonic units in the SE, the Verampio-Crevola section. This supports the burial hypothesis for explaining the origin of the concentric metamorphic zonation in the Central Alps as was postulated by NIGGLI (1970). However, this rapid uplift in the SE may have caused some important, late thermal effect as discussed by ENGLAND + RICHARDSON 1977. Uplift controlled by erosion will instantaneously bring about a decrease in pressure on a given rock, but a depth below a few

kilometers the temperature will substantially increase for some time before cooling starts. Such a late thermal effect (thermal dome), superimposed on the normal burial regime may have played a significant role in our cross-section contributing to the observed mineral textures and the local equilibrium-disequilibrium relations. Late recrystallization processes may have lowered drastically the permeability of the rock so that metamorphic fluids could not migrate any more and got trapped within local domains, restricting chemical equilibration to local domains (grain boundaries).

#### Acknowledgements

This study has benefited from many helpful discussions with M. Frey, E. Niggli, K. Hammer-schmidt, E. Jaeger and H. Schwander. I am highly indebted to K. Bucher, M. Frey and B. Vocke for critically reading and improving the manuscript. This work was supported in part by grants from the "Schweizerischer Nationalfonds" and by the foundation of DR. JOACHIM DE GIACOMI.

#### References

- AYRTON S. N. and RAMSAY J. G. 1974. Tectonic and Metamorphic Events in the Alps. *SMPM* 54, 609-639.
- BAILEY E. H. and STEVENS R. E. 1960. Selective staining of K-feldspar and plagioclase on rock slabs and thin sections. *Am. Miner.* 45, 1020-1025.
- BEARTH P. 1958. Über einen Wechsel der Mineralfacies in der Wurzelzone des Penninikums. *SMPM* 38, 363-373.
- BORG I. Y. and SMITH D. K. 1969. Calculated X-ray powder patterns for silicate minerals. *Geol. Soc. Am., Mem.* 122.
- BUCHER K., FRANK E. and FREY M. 1983. A model for the progressive regional metamorphism of margarite-bearing rocks in the Central Alps. *Am. J. Sci.* (in press).
- CHATTERJEE N. D. 1961. The alpine metamorphism in the Simplon Area, Switzerland and Italy. *Geol. Rundschau* 51, 1-72.
- CHATTERJEE N. D. 1974. Synthesis and upper thermal stability limit of 2M<sub>1</sub>-margarite CaAl<sub>2</sub>(Al<sub>2</sub>Si<sub>2</sub>O<sub>10</sub>/(OH)<sub>2</sub>). *SMPM* 54, 753-767.
- CHATTERJEE N. D. 1976. Margarite stability and compatibility relations in the system CaO-Al<sub>2</sub>O<sub>3</sub>-SiO<sub>2</sub>-H<sub>2</sub>O as a pressure-temperature indicator. *Am. Miner.* 61, 699-709.
- CRESSEY G., SCHMID R. and WOOD B. J. 1978. Thermodynamic properties of almandine-grossular garnet solid solutions. *Contr. Min. Petr.* 67, 397-404.
- DAHL P. S. 1979. Comparative geothermometry based on major element and oxygen isotope distributions in Precambrian metamorphic rocks from southwestern Montana. *Am. Miner.* 64, 1280-1293.
- DALLMEYER R. D. 1974. Metamorphic history of the Northeastern Reading Prong, New York and Northern New Jersey. *J. Petrology* 15, 325-359.
- ELLIS D. E. 1978. Stability and phase equilibria of chloride and carbonate bearing scapolites at 750 °C and 4000 bar. *Geochim. cosmochim. Acta* 42, 1271-1281.

- ENGLAND P. C. and RICHARDSON S. W. 1977. The influence of erosion upon the mineral facies of rocks from different metamorphic environment. *J. geol. Soc. Lond.* 134, 201-214.
- EUGSTER H. P., ALBEE A. L., BENICE A. E., THOMPSON J. B. and WALDBAUM D. R. 1972. The two-phase region and excess mixing properties of paragonite-muscovite crystalline solutions. *J. Petrology* 13, 147-179.
- EUGSTER H. P. and SKIPPEN G. B. 1967. Igneous and metamorphic reactions involving gas equilibria. In ABELSON P. H. *Research in geochemistry*, 2. New York, John Wiley & Sons, 492-520.
- ERNST W. G. 1973. Interpretative Synthesis of Metamorphism in the Alps. *Bull. geol. Soc. Am.* 84, 2053-2078.
- EVANS B. W. and GUIDOTTI C. V. 1966. The sillimanite-potash feldspar isograd in Western Maine, U.S.A. *Contr. Min. Petr.* 12, 25-62.
- EVANS B. D. and SHERMAN D. J. 1962. The application of chemical staining to the study of diagenesis in limestones. *Proc. geol. Soc. London* 10.
- FERRY J. M. and SPEAR F. S. 1978. Experimental calibration of the partitioning of Fe and Mg between biotite and garnet. *Contr. Miner. Petrol.* 66, 113-117.
- FOX J. S. 1975. Three-dimensional isograds from the Lukmanier Pass, Switzerland, and their tectonic significance. *Geol. Mag.* 112, 547-564.
- FRANK E. 1979. Metamorphose mesozoischer Gesteine im Querprofil Brig-Verampio: mineralogisch-petrographische und isotopengeologische Untersuchungen. Ph. D. thesis, University of Berne, pp. 204.
- FRANK E. and STETTLER A. 1979. K-Ar and  $^{39}\text{Ar}$ - $^{40}\text{Ar}$  systematics of white K-mica from an Alpine metamorphic profile in the Swiss Alps. *SMPM* 59, 375-394.
- FRENCH B. M. 1966. Some geological implications of equilibrium between graphite and a C-O-H gas phase at high temperatures and pressures. *Rev. Geophys.* 4, 223-253.
- FREY M. 1969. Die Metamorphose des Keupers vom Tafeljura bis zum Lukmanier-Gebiet. *Beitr. Geol. Karte Schweiz*, NF. 137.
- FREY M. and NIGGLI E. 1972. Margarite, an important rock-forming mineral in regionally metamorphosed low-grade rocks. *Naturwissenschaften* 59, 214-215.
- FREY M., HUNZIKER J., FRANK W., BOQUET J., DAL PIAZ G., JAEGER E. and NIGGLI E. 1974. Alpine metamorphism of the Alps, A Review. *SMPM* 54, 247-290.
- FREY M. and ORVILLE P. 1974. Plagioclase in margarite-bearing rocks. *Amer. J. Sci.* 274, 31-47.
- FREY M., BUCHER K., FRANK E. and SCHWANDER H. 1982. Margarite in the Central Alps. *SMPM* 62, 21-45.
- GHENT E. D. 1976. Plagioclase-garnet- $\text{Al}_2\text{SiO}_5$ -quartz: a potential geobarometer-geothermometer. *Am. Miner.* 61, 710-714.
- GHENT E. D., ROBBINS D. B. and STOUT M. Z. 1979. Geothermometry, geobarometry and fluid compositions of metamorphosed calc-silicates and pelites, Mica Creek, British Columbia. *Am. Miner.* 64, 874-885.
- GOLDMAN D. S. and ALBEE A. L. 1977. Correlation of Mg/Fe partitioning between garnet and biotite with  $^{18}\text{O}/^{16}\text{O}$  partitioning between quartz and magnetite. *Amer. J. Sci.* 277, 750-767.
- GOLDSMITH J. R. and LAVES F. 1954. The microcline-sanidine stability relations. *Geochim. cosmochim. Acta* 5, 1-19.
- GOLDSMITH J. R. and NEWTON R. C. 1977. Scapolite-plagioclase stability relations at high pressures and temperatures in the system  $\text{NaAlSi}_3\text{O}_8$ - $\text{CaAl}_2\text{Si}_2\text{O}_8$ - $\text{CaCO}_3$ - $\text{CaSO}_4$ . *Amer. Miner.* 62, 1063-1081.
- GREW E. 1974. Carbonaceous material in some metamorphic rocks of New England and other areas. *J. Geol.* 82.
- GUIDOTTI C. V. 1970. The mineralogy and petrology of the transition from the lower to upper sillimanite zone in the Oquossoc area, Maine, *J. Petrology* 11, 277-336.
- GUIDOTTI C. V. and SASSI F. 1976. Muscovite as a petrogenetic indicator mineral in metamorphosed pelites and semipelites. *N. Jb. Miner. Abh.* 127, 97-142.

- HALL W. D. M. 1972. The structural and metamorphic history of the lower pennine nappes, Valle di Bosco, Ticino, Switzerland. Ph. D. thesis, London University.
- HELGESON H. C., DELANY J. M., NESBITT H. H. and BIRD D. K. 1978. Summary and critique of the thermodynamic properties of rock-forming minerals. *Amer. J. Sci.* 278-A.
- HEWITT D. A. 1973. Stability of the assemblage muscovite-calcite-quartz. *Am. Miner.* 58, 785-791.
- HEY M. H. 1954. A new review of the chlorites. *Min. Mag.* 30, 277-292.
- HOLDAWAY M. J. 1971. Stability of andalusite and the aluminium silicate phase diagram. *Amer. J. Sci.* 271, 97-131.
- HUNZIKER J. and BEARTH P. 1969. Rb-Sr-Altersbestimmungen aus den Walliser Alpen. Biotit-Alterswerte und ihre Bedeutung für die Abkühlungsgeschichte der alpinen Metamorphose. *Eclogae geol. Helv.* 62, 205-222.
- JAEGER E., NIGGLI E. and WENK E. 1967. Rb-Sr Altersbestimmungen an Glimmern der Zentralalpen. *Beitr. geol. Karte Schweiz, NF.* 134.
- JAEGER E. 1973. Die alpine Orogenese im Lichte radiometrischer Altersbestimmungen. *Eclogae geol. Helv.* 66, 11-21.
- KÖPPEL V. and GRÜNENFELDER M. 1978. The significance of monazite U-Pb ages; examples from the Lepontine area of the Swiss Alps. 4<sup>th</sup> Int. Conf. Geochronology, Cosmochronology and Isotope Geology, U.S. Geol. Survey Open File Report, 78-701.
- KWAK T.A.P. 1968. Ti in biotite and muscovite as an indicator of metamorphic grade in almandine amphibolite facies rocks from Sudbury, Ontario. *Geochim. cosmochim. Acta* 32, 1222-1229.
- LANDIS C. A. 1971. Graphitization of dispersed carbonaceous material in metamorphic rocks. *Contr. Miner. Petrol.* 30, 30-45.
- LEAKE B. E. 1978. Nomenclature of amphiboles. *Am. Miner.* 63, 1023-1052.
- MILNES A. G. 1973. Structural reinterpretation of the classic Simplon tunnel section of the Central Alps. *Bull. Geol. Soc. Am.* 84, 269-274.
- MILNES A. G. 1974. Post-nappe folding in the western Lepontine Alps. *Eclogae geol. Helv.* 67, 333-348.
- NIGGLI E. 1970. Alpine Metamorphose und alpine Gebirgsbildung. *Fortschr. Mineralogie* 47, 16-26.
- NIGGLI E. und NIGGLI C. 1965. Karten der Verbreitung einiger Mineralien der alpidischen Metamorphose in den Schweizer Alpen (Stilpnomelan, Alkali-Amphibol, Chloritoid, Staurolith, Disthen, Sillimanit). *Eclogae geol. Helv.* 58, 335-368.
- NITSCH K. H. und STORRE B. 1972. Zur Stabilität von Margarit in H<sub>2</sub>O-CO<sub>2</sub>-Gasgemischen. *Fortschr. Miner.* 50, 71-73.
- OTERDOOM W. H. 1979. Plagioclase-scapolite-calcite phase relations in high-metamorphic argillaceous limestones. *SMPM* 59, 417-421.
- PLAS VAN DER L. 1959. Petrology of the northern Adula region, Switzerland. *Leidse geol. Meded.* 24, 415-598.
- POTY B. P., STALDER H. A. and WEISBROD A. M. 1974. Fluid inclusions studies in quartz from fissures of Western and Central Alps. *SMPM* 54, 717-752.
- PURDY J. W. and JAEGER E. 1976. K-Ar ages on rock-forming minerals from the Central Alps. *Mem. Inst. Geol. Min. Univ. Padova*, XXX.
- RICHARDSON S. W., GILBERT M. C. and BELL P. M. 1969. Experimental determination of kyanite-andalusite and andalusite-sillimanite equilibria: the aluminium silicate triple point. *Amer. J. Sci.* 267, 259-272.
- ROSENFELD J. L. 1969. Stress effects around quartz inclusions in almandine and the piezothermometry of coexisting aluminium silicates. *Amer. J. Sci.* 267, 317-351.
- SCHWANDER H. and GLOOR F. 1980. Zur quantitativen Mikrosondenanalyse von geologischen Proben mittels kombiniertem EDS-WDS. X-ray Spectrom. 9/3, 134-137.

- SHAW D. M. 1960. The geochemistry of scapolite. Part 1. Previous work and general mineralogy. *J. Petrology* 1, 218-260.
- SHENGELIA D. M., AKHVLEDIANI R. A. and KETSKHOVELI D. N. 1977. The graphite geothermometer. *Doklady Akad. Nauk. SSSR* Vol. 235, 132-134.
- SLAUGHTER J., KERRICK D. M. and VALL V. J. 1975. Experimental and thermodynamic study of equilibria in the system  $\text{CaO-MgO-SiO}_2\text{-H}_2\text{O-CO}_2$ . *Amer. J. Sci.* 275, 143-162.
- STECK A., RAMSAY J. G., MILNES A. G. and BURRI M. 1979. *Compte rendu de l'excursion de la Société géologique suisse et la Société de Minéralogie et Petrographie en Valais et en Italie du Nord, du 2 au 5 octobre 1978.* *Eclogae geol. Helv.* 72/1.
- STRECKEISEN A. and WENK E. 1974. On steep isogradic surfaces in the Simplon area. *Contr. Miner. Petrol.* 47, 81-95.
- THOMPSON A. B. 1974. Calculation of muscovite-paragonite-alkali feldspar phase relations. *Contr. Min. Petrol.* 44, 173-194.
- THOMPSON A. B. 1976. Mineral reactions in pelitic rocks: I Prediction of P-T-X (Fe-Mg) phase relations. *Amer. J. Sci.* 276, 401-424.
- TROMMSDORFF V. 1966. Progressive Metamorphose kieseliger Karbonatgesteine in den Zentralalpen zwischen Bernina und Simplon. *SMPM* 46, 431-460.
- TRÜMPY R. 1960. Paleotectonic evolution of the Central and Western Alps. *Bull. geol. Soc. Am.* 71, 843-908.
- TRÜMPY R. 1980. *Geology of Switzerland. Part A: An outline of the geology of Switzerland.* Wepf & Co., Publishers, Basel, New York.
- VELDE B. 1965. Phengite micas: synthesis, stability and natural occurrence. *Amer. J. Sci.* 263, 886-913.
- WENK E. 1962. Plagioklas als Indexmaterial in den Zentralalpen. *SMPM* 42, 139-153.
- WENK E. 1969. Zur Regionalmetamorphose und Ultrametamorphose im Lepontin. *Fortschr. Mineral.* 47, 34-51.
- ZEN E-AN and ALBEE A. L. 1964. Coexisting muscovite and paragonite in pelitic schists. *Am. Miner.* 49, 904-925.

Manuscript received 21 Decembre, 1982.

## APPENDIX

Table 1 Mineral assemblages of 23 samples used for mineral analyses by microprobe technique.

	mu	ma	pa	bi	chl	ga	am	st	zo	plg	kf	sc	ky	co	qz	cc	dol	g	tc
EF 627	●	○	○		●					●					●	●			●
EF 938	●				●				●	●					●	●			●
EF 40	●	●		●	●				●	●					●	●			●
EF 42	●	○	●	○					○	●					●	●			●
EF 137					●		●								●	●	●		●
EF 170	●	●		●	●	●	●		●	●					●	●			●
EF 211	●		●	●	○	●			●	●					●	○			●
EF 227	●	●		●					●	●					●	○			●
EF 355	●			●	●	○	●		●	●					●	○			●
EF 271	●	●		●	○	●		●	●	●			●		●				●
S 7010	○		●	○		●		●	●	●			●		●				●
EF 440	●	●		●	●				●	●					●				●
EF 806	●			●	○	●			●	●					●	○			●
EF 766				●	●		●		●	○			●		○	○	○		●
EF 853	●			●	●	●		●	●	●					●	○	○		●
EF 736	●			●	●	●		●	●	●			○		●	○	○		●
EF 741	●			●	●	●		●	●	●					●	○	○		●
EF 660	●			●	●	●			●	●	●				●	●			●
EF 869	●	●		●	○	●			●	●	●	●	○	●	●	●			●
EF 870	●	●		●	●	●			●	●	●	●	○	●	●	●			●
EF 876	●			●	○	●		○	●	●					●				●
EF 920	●			●	○	●			●	●	●	●		○	●	●			●
EF 922	●			●	○	●			●	●	●	●			●	●			●

metamorphic grade →

○ traces

## Abbreviations for mineral names:

am = amphibole	dol = dolomite	ma = margarite	sc = scapolite
bi = biotite	g = graphite	mu = muscovite	st = staurolite
cc = calcite	ga = garnet	pa = paragonite	tc = talc
chl = chlorite	kf = k-feldspar	plg = plagioclase	zo = zoisite
co = corundum	ky = kyanite	qz = quartz	

Table 2 Chemical composition of muscovite.

margarite and paragonite														
sample	EF	170	227	440	440	440	870	870	870	42	42	42	211	211
SiO <sub>2</sub>	30.80	32.53	31.04	31.59	31.60	30.80	30.61	33.56	45.30	46.40	46.10	46.20	45.14	
Al <sub>2</sub> O <sub>3</sub>	49.50	48.79	50.77	50.53	49.61	49.68	49.83	47.11	40.30	39.98	40.36	38.90	40.26	
TiO <sub>2</sub>	.20	.13	.10	.10	.19	-	-	-	-	-	.14	.12	-	
FeO	.35	.83	.30	.47	.21	.20	.30	.20	-	.20	.18	.66	.30	
MgO	.20	.38	-	.39	.10	.10	.10	.39	.30	.10	.10	.32	.16	
MnO	-	-	-	-	-	-	-	-	-	-	-	-	-	
CaO	10.80	10.34	12.20	11.61	10.50	12.35	12.76	11.41	.59	.42	.38	.44	.80	
Na <sub>2</sub> O	1.45	1.68	1.00	1.23	1.60	.80	.73	.91	7.21	6.80	6.94	5.86	6.71	
K <sub>2</sub> O	.21	.35	-	.09	.20	.10	-	.81*	.98	1.20	.80	2.34	1.08	
anhydrous total	93.50	95.03	95.39	96.00	94.01	94.03	94.32	94.38	94.67	95.10	95.00	94.84	94.45	
number of ions on the basis of 22(O)														
Si	4.16	4.32	4.11	4.15	4.23	4.14	4.10	4.48	5.84	5.94	5.91	5.98	5.84	
Al	3.84	3.68	3.89	3.85	3.77	3.86	3.90	3.52	2.16	2.06	2.09	2.02	2.16	
Al	4.03	3.96	4.02	3.98	4.05	4.00	3.97	3.89	3.97	3.98	4.01	3.91	3.99	
Ti	.02	.01	.01	.01	.02						.01	.01		
Fe	.03	.09	.03	.05	.02	.02	.03	.02		.02	.02	.07	.03	
Mg	.04	.07		.08	.02	.02	.02	.08	.06	.02	.02	.06	.03	
Mn														
Ca	1.56	1.47	1.73	1.63	1.50	1.78	1.84	1.63	.08	.06	.05	.06	.11	
Na	.37	.43	.26	.31	.41	.21	.19	.23	1.80	1.69	1.72	1.47	1.69	
K	.03	.04		.01	.03	.02		.14	.16	.20	.13	.38	.17	

\*intergrowth with muscovite

Table 3 Chemical composition of margarite and paragonite.

Representative microprobe analyses of muscovite														
sample	170	273	273	65	65	440	440	806	806	853	853	736	660	660
SiO <sub>2</sub>	47.45	48.18	46.70	47.20	47.22	46.30	47.70	46.80	46.21	45.59	45.62	46.01	47.80	46.58
Al <sub>2</sub> O <sub>3</sub>	34.38	32.20	34.98	35.63	35.34	34.10	31.60	34.80	35.30	34.83	34.80	34.90	33.60	33.32
TiO <sub>2</sub>	.26	.18	.57	.60	.30	.42	.30	.60	.51	.67	.94	.81	.63	.77
FeO	1.33	1.30	1.06	.80	1.05	.98	1.30	1.23	1.10	1.07	1.04	.87	1.54	1.93
MgO	1.48	1.95	1.18	1.25	1.43	1.10	2.20	1.08	1.00	1.15	1.22	1.38	1.61	1.57
MnO														
CaO							.10							
Na <sub>2</sub> O	1.28	.68	1.36	.80	.63	1.75	.50	.50	.43	1.00	.89	.79	.23	.30
K <sub>2</sub> O	9.50	10.65	9.59	10.10	9.80	10.50	10.48	11.00	11.10	10.18	10.24	10.30	11.29	10.30
anhydrous total	95.68	95.13	95.44	96.38	95.77	94.15	94.18	96.00	95.64	94.49	94.75	95.06	96.47	95.76
number of ions on the basis of 22(O)														
Si	6.26	6.42	6.18	6.18	6.21	6.23	6.42	6.20	6.14	6.12	6.11	6.13	6.30	6.22
Al	1.74	1.58	1.82	1.82	1.79	1.77	1.58	1.80	1.86	1.88	1.89	1.87	1.70	1.78
Al	3.60	3.48	3.64	3.66	3.69	3.64	3.44	3.62	3.67	3.63	3.60	3.61	3.52	3.47
Ti	.03	.02	.06	.06	.03	.04	.03	.06	.05	.07	.09	.08	.06	.08
Fe	.17	.14	.12	.09	.12	.11	.15	.14	.12	.12	.12	.10	.32	.21
Mg	.29	.39	.23	.24	.28	.22	.44	.21	.20	.23	.24	.27	.17	.31
Mn														
Ca							.01							
Na	.33	.18	.35	.20	.16	.20	.13	.13	.11	.26	.23	.20	.08	.08
K	1.60	1.81	1.62	1.69	1.65	1.80	1.80	1.86	1.88	1.74	1.75	1.75	1.90	1.93

Table 4 Chemical composition of biotite.

Biotite														
sample	170	170	355	355	273	273	65	65	660	660	869	869	920	920
SiO <sub>2</sub>	36.70	37.27	36.35	35.00	37.10	36.71	37.60	37.20	37.50	36.47	36.53	35.70	37.89	36.80
Al <sub>2</sub> O <sub>3</sub>	19.29	18.55	19.70	18.90	18.00	18.04	18.42	18.46	18.50	18.75	18.51	18.30	17.84	17.55
TiO <sub>2</sub>	1.66	1.53	1.70	1.30	1.55	1.40	1.62	1.53	2.89	2.57	2.84	3.35	2.78	2.70
FeO	15.68	16.28	16.80	17.60	16.90	17.40	13.70	13.46	16.51	20.74	16.70	19.30	11.39	11.20
MgO	12.35	12.34	10.83	12.34	12.96	12.52	14.81	14.51	10.54	7.74	10.41	8.70	15.15	14.60
MnO	.17	.16										.11		
CaO	.30													
Na <sub>2</sub> O	.15	.17	.10	.21	.10	.10	.10	.10						
K <sub>2</sub> O	9.55	9.36	9.60	9.00	9.54	9.40	9.10	9.20	10.41	10.17	10.10	9.86	10.25	10.40
anhydrous total	95.85	95.66	95.08	94.45	96.15	95.56	95.35	94.46	96.35	96.44	95.09	95.32	95.30	93.31
number of ions on the basis of 22(O)														
Si	5.44	5.54	5.46	5.33	5.51	5.50	5.53	5.52	5.57	5.52	5.51	5.44	5.55	5.53
Al	2.56	2.46	2.54	2.67	2.49	2.50	2.47	1.48	2.43	2.48	2.49	2.56	2.45	2.47
Al	.81	.79	.95	.72	.66	.69	.72	.75	.81	.87	.80	.73	.63	.63
Ti	.18	.17	.19	.15	.17	.16	.18	.17	.32	.29	.32	.38	.31	.30
Fe	1.95	2.02	2.11	2.24	2.10	2.18	1.68	1.67	2.33	1.75	2.10	2.46	1.40	1.41
Mg	2.73	2.74	2.42	2.80	2.87	2.80	3.24	3.21	2.05	2.63	2.34	1.98	3.31	3.27
Mn	.02	.02										.01		
Ca	.05													
Na	.04	.04	.03	.03	.03	.03	.03	.03						
K	1.81	1.78	1.84	1.75	1.81	1.80	1.71	1.74	1.97	1.96	1.94	1.92	1.91	1.99

Table 5 Chemical composition of chlorite.

Chlorite											
sample	627	627	41	41	170	170	853	853	869	869	870
SiO <sub>2</sub>	24.96	25.80	24.86	24.10	24.36	23.65	23.04	23.50	24.45	23.26	24.52
Al <sub>2</sub> O <sub>3</sub>	22.70	21.96	23.10	22.60	23.05	22.36	22.06	21.97	23.10	21.35	23.20
TiO <sub>2</sub>	.20								.13		.15
FeO	20.32	20.30	22.87	22.85	21.98	24.64	23.80	27.85	22.24	21.67	22.10
MgO	17.00	17.60	17.15	16.61	17.32	16.12	14.01	13.78	15.32	14.23	15.50
MnO									.18	.19	.20
CaO				.27					.14	.19	.19
Na <sub>2</sub> O											
K <sub>2</sub> O							.10	.10		.15	
anhydrous total	85.18	85.00	87.98	86.43	86.71	86.77	83.01	87.34	85.61	81.02	85.86
number of ions on the basis of 28(O)											
Si	5.26	5.30	5.15	5.10	5.10	5.04	5.12	5.07	5.20	5.25	5.19
Al	2.74	2.70	2.85	2.90	2.90	2.96	2.88	2.93	2.80	2.75	2.81
Al	2.90	2.78	2.81	2.74	2.79	2.65	2.89	2.65	2.99	2.93	2.98
Ti	.02										
Fe	3.58	3.60	3.96	4.04	3.85	4.39	4.43	5.02	3.95	4.09	3.91
Mg	5.34	5.56	5.29	5.24	5.41	5.12	4.64	4.43	4.85	4.79	4.89
Mn									.03	.04	.04
Ca				.06					.03	.04	.04
Na											
K							.03	.03		.04	

Table 6 Chemical composition of garnet.

Garnet														
sample	170 <sub>r</sub>	170 <sub>c</sub>	65 <sub>r</sub>	65 <sub>c</sub>	853 <sub>r</sub>	853 <sub>c</sub>	660 <sub>r</sub>	660 <sub>c</sub>	922 <sub>r</sub>	922 <sub>c</sub>	870 <sub>r</sub>	870 <sub>c</sub>	876 <sub>r</sub>	876 <sub>c</sub>
SiO <sub>2</sub>	37.90	37.03	37.89	37.53	37.43	37.07	37.98	37.30	37.79	37.54	37.43	37.68	37.73	37.76
Al <sub>2</sub> O <sub>3</sub>	21.88	21.30	21.56	21.50	21.85	21.32	21.71	21.68	22.06	21.87	21.70	21.40	21.45	21.20
TiO <sub>2</sub>														
FeO	28.83	24.66	30.30	25.52	31.20	30.77	27.48	27.83	28.16	29.15	31.44	31.45	30.72	30.23
MgO	3.04	1.26	2.91	1.62	4.11	2.36	2.50	2.52	3.30	2.70	2.25	1.67	2.84	1.49
MnO	2.28	7.92	0.88	7.40	0.17	1.31	0.87	1.20	0.22	0.66	1.11	0.40	0.21	1.22
CaO	7.03	7.81	7.03	7.42	5.50	6.57	10.10	9.84	8.93	8.95	6.90	7.47	7.49	8.93
anhydrous total	100.9	99.9	100.5	100.9	100.2	99.4	100.6	100.3	100.4	100.8	100.8	100.1	100.4	100.8
Number of ions on the basis of 24(O)														
Si	5.96	5.95	5.99	5.96	5.92	5.96	5.97	5.91	5.93	5.92	5.94	6.00	5.98	5.99
Al	.04	.05	.01	.04	.08	.04	.03	.09	.07	.08	.06		.02	.01
Al	4.01	3.99	4.00	3.99	3.99	4.00	3.99	3.96	4.01	3.98	4.00	4.02	3.99	3.96
Fe	3.79	3.31	4.00	3.39	4.13	4.14	3.61	3.69	3.70	3.84	4.17	4.19	4.07	4.01
Mg	.71	.30	.68	.39	.97	.57	.59	.59	.77	.63	.53	.40	.67	.35
Mn	.30	1.08	.12	1.00	.02	.18	.12	.16	.03	.08	.15	.05	.03	.16
Ca	1.18	1.34	1.19	1.26	.93	1.13	1.70	1.67	1.50	1.51	1.17	1.28	1.27	1.52
Alm	63.38	54.88	66.80	56.17	68.20	68.80	60.05	60.27	61.61	63.23	69.20	70.80	67.40	66.40
Pyr	11.87	4.99	11.40	6.40	16.01	9.40	9.73	9.72	12.86	10.43	8.80	6.70	11.10	5.80
Gross	19.73	22.26	19.90	20.93	15.40	18.82	28.27	27.36	25.03	24.87	19.50	21.60	21.00	25.20
Spess	5.01	17.85	1.90	16.50	.37	2.96	1.92	2.73	.48	1.45	2.50	.80	.50	2.60

r=rim ; c=core

Table 7 Chemical composition of Ca-amphibole.

Ca-amphibole													
sample	137	137	137	170	170	170	355	355	355	355	274	274	274
SiO <sub>2</sub>	54.20	54.40	54.19	42.55	41.95	42.01	42.70	42.20	42.00	41.53	42.11	42.86	41.80
Al <sub>2</sub> O <sub>3</sub>	5.82	5.60	5.90	17.70	17.60	17.19	17.30	18.10	18.20	18.35	17.43	17.46	17.21
TiO <sub>2</sub>	.14	.14	.10	.25	.50	.50	.48	.40	.35	.36	.31	.51	.32
FeO	.68	1.04	.97	14.94	15.05	15.10	15.09	16.95	16.81	16.38	18.42	18.60	18.80
MgO	21.77	21.85	21.80	8.61	8.83	8.58	8.98	8.30	8.27	8.16	7.48	7.64	7.38
MnO										.20	.31	.30	.16
CaO	12.75	12.81	12.98	11.00	10.93	10.75	11.10	10.90	11.13	11.05	10.14	10.01	10.22
Na <sub>2</sub> O	.71	.60	.70	1.77	1.74	1.71	1.43	1.50	1.63	1.40	1.82	1.80	1.83
K <sub>2</sub> O	.12	.10	.11	1.84	1.86	1.89	1.86	2.08	2.06	2.03	2.28	2.29	2.34
F		.20	.20										
anhydrous total	96.18	96.65	96.75	97.22	97.06	96.10	97.40	98.81	98.77	97.84	98.56	98.88	98.10
number of ions on the basis of 23(O)													
Si	7.49	7.49	7.46	6.28	6.22	6.27	6.29	6.18	6.16	6.13	6.24	6.22	6.23
Al	.51	.51	.54	1.72	1.78	1.73	1.71	1.82	1.84	1.87	1.76	1.78	1.77
Al	.44	.49	.41	1.36	1.29	1.30	1.29	1.30	1.31	1.33	1.28	1.28	1.25
Ti	.01	.01	.01	.03	.06	.06	.05	.05	.04	.04	.03	.06	.04
Fe	.08	.12	.11	1.84	1.86	1.89	1.86	2.08	2.06	2.03	2.28	2.29	2.34
Mg	4.49	4.48	4.47	1.89	1.95	1.91	1.97	1.81	1.81	1.80	1.65	1.68	1.63
Mn										.02	.03	.04	.02
Na	.19	.16	.19	.51	.50	.49	.41	.43	.46	.40	.52	.52	.53
Ca	1.89	1.89	1.91	1.74	1.73	1.72	1.75	1.71	1.75	1.75	1.61	1.58	1.63
K	.02	.02	.02	.07	.09	.07	.07	.09	.07	.08	.08	.07	.07
F		.09	.09										
rock type	siliceous dolomite/ calcareous schists(schistes lustrés)												

Table 8 Chemical composition of zoisite-clinozoisite.

zoisite-clinozoisite												
sample	355	355	440	440	806	806	650	650	869	870	870	920
SiO <sub>2</sub>	39.34	39.40	38.94	39.23	39.30	39.42	38.40	37.91	38.97	37.60	38.61	39.40
Al <sub>2</sub> O <sub>3</sub>	29.23	29.71	30.46	29.83	30.31	32.40	29.25	29.51	31.12	30.05	31.12	32.12
Fe <sub>2</sub> O <sub>3</sub>	5.85	5.98	4.13	6.00	4.67	2.01	6.01	5.22	1.98	2.75	1.12	1.30
MgO				.22			.44	.30				.30
CaO	23.90	24.12	23.26	23.55	24.00	24.35	24.03	23.90	24.05	24.80	24.60	24.48
anhydrous total	98.32	99.21	96.79	98.83	98.28	98.18	98.13	96.83	96.63	95.20	95.45	97.59
number of ions on the basis of 12.5(O)												
Si	3.02	3.00	3.02	3.00	3.00	3.00	2.97	2.96	3.01	2.97	3.02	3.01
Al							.03	.04		.03		
Al <sub>IV</sub>	2.65	2.67	2.78	2.69	2.74	2.90	2.64	2.68	2.88	2.78	2.87	2.89
Fe <sup>+3</sup>	.34	.34	.24	.34	.27	.11	.35	.31	.11	.16	.07	.07
Mg				.02			.05	.03				.03
Ca	1.97	1.97	1.93	1.93	1.97	1.98	1.99	2.00	1.99	2.10	2.06	2.00

Table 9 Chemical composition of K-feldspar.

k-feldspar										
sample	660 <sub>a</sub>	660 <sub>a</sub>	660 <sub>a</sub>	660 <sub>b</sub>	869	869	870	870	920	920
SiO <sub>2</sub>	65.60	65.59	65.74	64.06	64.10	65.80	64.62	65.59	64.10	64.60
Al <sub>2</sub> O <sub>3</sub>	18.30	18.81	18.29	19.00	19.29	18.80	18.37	18.31	19.00	18.65
CaO	.10	.05	.11	.24	.26	.03		.10	.24	
Na <sub>2</sub> O	1.19	.84	1.20	.66	1.34	.84	.87	1.18	.66	.70
K <sub>2</sub> O	15.20	15.70	15.43	15.55	14.90	15.50	15.33	15.22	15.55	15.64
total	100.39	100.99	100.77	99.51	99.89	100.97	99.19	100.40	99.55	99.59
Or	89.2	92.3	89.4	92.9	87.4	92.4	92.1	89.2	92.8	93.6
Ab	10.4	7.5	10.5	6.0	11.5	7.5	7.9	10.4	6.0	6.4
An	.4	.2	.1	1.1	1.1	.1		.4	1.2	

Table 10 Chemical composition of scapolite.

Scapolite									
sample	660a	660a	660b	660b	869	869	870	870	869
SiO <sub>2</sub>	46.82	45.50	45.80	46.20	45.61	46.30	46.30	46.20	44.74
Al <sub>2</sub> O <sub>3</sub>	28.23	27.80	27.90	27.91	28.40	27.80	28.01	27.90	28.19
FeO									
MgO			.30	.19	.25	.20	.30	.30	
CaO	18.45	18.65	18.20	18.10	18.36	18.61	18.30	18.20	19.34
Na <sub>2</sub> O	2.98	2.89	3.20	3.30	3.11	3.09	3.00	3.19	2.81
K <sub>2</sub> O		.05			.10				.05
Cl			tr	tr					
anhydrous total	96.48	94.89	95.40	95.70	95.83	96.00	95.91	95.79	95.13
number of ions on the basis of 12(Si + Al)									
Si	7.02	6.98	6.99	7.01	6.92	7.03	7.01	7.01	6.89
Al	4.98	5.02	5.01	4.99	5.08	4.97	4.99	4.99	5.11
Mg			.07	.04	.06	.04	.07	.07	
Ca	2.96	3.06	2.97	2.94	2.98	3.02	2.97	2.96	3.19
Na	.87	.86	.95	.97	.91	.91	.88	.94	.83
K		.01			.02				.01
EqAn <sub>x</sub> *	66.00	67.33	67.00	66.33	69.33	65.67	66.33	66.33	70.33
Mei <sup>**</sup>	77.30	77.86	75.76	75.19	76.21	76.84	77.10	75.90	79.16

\* ELLIS (1978)

\*\* SHAW (1960)

Table 11 Chemical composition of staurolite.

Microprobe analyses of staurolite						
sample	EF 853	EF 736/1	736/2	736/3	736/4 <sub>rim</sub>	736/4 <sub>core</sub>
SiO <sub>2</sub>	28.14	28.60	27.67	28.61	28.57	29.08
Al <sub>2</sub> O <sub>3</sub>	54.76	53.77	53.00	53.92	53.89	54.05
TiO <sub>2</sub>	.72	.59	.66	.48	.82	.55
FeO	10.91	10.72	10.08	10.76	10.87	10.71
MnO		.10	.19			
MgO	1.47	1.79	1.44	1.91	1.93	1.67
ZnO	1.72	2.08	2.11	2.40	2.04	2.07
anhydrous total	97.72	97.66	95.16	98.09	98.11	98.13
number of ions on the basis of 46(O)						
Si	7.76	7.91	7.84	7.89	7.86	7.99
Al	17.80	17.52	17.70	17.51	17.48	17.49
Ti	.15	.12	.14	.10	.16	.11
Fe	2.51	2.48	2.39	2.48	2.50	2.46
Mg	.60	.74	.61	.78	.79	.68
Mn		.02	.04			
Zn	.35	.42	.44	.49	.42	.42
Mg/Mg+Fe	.193	.230	.203	.239	.240	.217

Table 12 Chemical composition of corundum.

microprobe analyses of corundum							
SiO <sub>2</sub>	.10	.28	.16	.15	.25	.26	.12
Al <sub>2</sub> O <sub>3</sub>	98.85	98.86	98.96	99.08	98.65	98.78	98.87
FeO <sub>tot</sub>	.15	.19	.18	.37	.45	.43	.43
TiO <sub>2</sub>	.05	.05	-	-	.08	.05	-
Cr <sub>2</sub> O <sub>3</sub>	.10	-	-	-	.04	-	-
total	99.25	99.38	99.30	99.60	99.47	99.52	99.42

Table 13 Chemical composition of calcite.

Calcite														
sample	627	627	41	41	41	355	355	806	806	806	660	660	869	869
FeCO <sub>3</sub>	3.772	3.892	4.078	3.901	2.821	4.420	4.236	3.484	3.710	3.226	2.145	2.486	2.321	2.047
MnCO <sub>3</sub>	1.993	.721	.324	.518	.243	.990	.908	.340	.486	.373	.243	.252	1.037	1.030
MgCO <sub>3</sub>	3.326	3.437	3.849	2.971	2.301	3.912	3.600	3.535	4.058	2.720	1.275	1.976	1.820	1.757
CaCO <sub>2</sub>	92.05	92.45	92.67	93.06	95.62	92.06	92.18	93.13	93.00	93.85	96.62	95.87	95.65	95.51
total	100.1	100.5	100.9	100.4	100.9	101.3	100.9	100.4	101.2	100.1	100.2	100.5	100.8	100.3

Table 14 Plagioclase and garnet compositions and estimates of pressure.

Calcium partitioning between coexisting plagioclase and garnet (rim) (GHENT 1976)

sample	T(°C)	x <sup>plag</sup> <sub>An</sub>	x <sup>garnet</sup> <sub>Gr</sub>	log K <sub>D</sub>	log K <sub>D</sub> +log K <sub>Y</sub>	pressure(kb)
273	510	.580	.210	-1.324	-1.724	6.0
		.501	.211	-1.130	-1.530	6.5
		.500	.230	-1.013	-1.413	6.8
701	520	.210	.102	-.941	-1.341	6.7
		.190	.070	-1.301	-1.701	5.9
		.181	.074	-1.158	-1.538	6.2
		.191	.080	-1.127	-1.527	6.3
		.220	.078	-1.351	-1.751	5.8
806	530	.547	.189	-1.380	-1.780	5.9
		.525	.188	-1.334	-1.734	6.0
		.477	.190	-1.196	-1.596	6.3
853	550	.490	.171	-1.372	-1.772	6.3
		.440	.183	-1.143	-1.543	6.9
		.580	.154	-1.728	-2.128	5.5
		.390	.151	-1.236	-1.636	6.7
		.350	.154	-1.069	-1.469	7.0
		.371	.165	-1.052	-1.452	7.1
		.400	.155	-1.235	-1.635	6.6
		.480	.160	-1.431	-1.831	6.2
736	550	.518	.172	-1.436	-1.836	6.2
		.520	.185	-1.356	-1.746	6.4
		.463	.175	-1.268	-1.668	6.6
		.470	.167	-1.348	-1.748	6.4
		.525	.184	-1.366	-1.766	6.3
		.501	.155	-1.526	-1.926	6.0
869	590	.764	.213	-1.666	-2.066	6.4
		.668	.223	-1.430	-1.830	6.9
		.672	.191	-1.639	-2.039	6.4
		.752	.212	-1.650	-2.050	6.4
870	590	.870	.197	-1.938	-2.338	5.7
		.930	.203	-1.983	-2.383	5.6
		.921	.197	-2.010	-2.410	5.5
		.980	.204	-2.045	-2.445	5.4
		.570	.200	-1.366	-1.766	7.1
		.841	.228	-1.700	-2.100	6.3
		.863	.239	-1.800	-2.200	6.0
.812	.197	-1.847	-2.247	5.9		
922	590	.510	.213	-1.137	-1.537	7.5
		.607	.249	-1.161	-1.561	7.4
		.538	.256	-.568	-1.368	7.8
		.498	.203	-1.176	-1.576	7.3

Table 15 Garnet and biotite compositions and estimates of temperature.

Mg/Fe partitioning between coexisting garnet (rim) and biotite

sample	(Mg/Fe) <sub>ga</sub>	(Mg/Fe) <sub>bi</sub>	K <sub>D</sub>	ln K <sub>D</sub>	T <sub>1</sub> <sup>*</sup>	$\bar{T}$	s.dev.
EF 170	.1878	1.1820	.1589	-1.839	538 (4kb)		
	.1669	1.285	.1299	-2.041	480		
	.1668	1.238	.1347	-2.004	480		
	.1369	1.149	.1191	-2.127	458		
	.1680	1.134	.1481	-1.909	517		
	.1763	1.084	.1626	-1.816	546		
	.1709	1.247	.1370	-1.987	495		
	.1487	1.232	.1207	-2.114	448	465°C	45
	.1632	1.405	.1162	-2.153	439		
	.1469	1.403	.1047	-2.257	414		
	.1430	1.393	.1027	-2.276	410		
	.1623	1.350	.1202	-2.119	448		
	.1374	1.362	.1008	-2.294	406		
	.1521	1.390	.1094	-2.212	437		
EF 165	.1084	.9419	.1151	-2.162	450		
	.1420	.9293	.1528	-1.878	528		
	.1250	.9356	.1338	-2.011	489	511	36
	.1466	.9203	.1593	-1.837	539		
	.1472	.9085	.1620	-1.820	545		
	.1361	.9289	.1465	-1.921	514		
EF 65	.1767	1.9790	.0893	-2.416	395		
	.2177	2.0491	.1062	-2.242	434		
	.2060	1.9500	.1056	-2.248	432		
	.2457	2.0661	.1189	-2.129	461		
	.1518	2.0132	.0754	-2.584	362		
	.2347	1.8941	.1239	-2.088	472	421	41
	.2386	1.9930	.1197	-2.122	463		
	.1432	1.9540	.0728	-2.630	355		
	.1998	1.8790	.1063	-2.241	434		
	.1715	1.8370	.0934	-2.371	405		
EF 440	.1736	1.8365	.0945	-2.358	407		
	.1421	1.7200	.0826	-2.493	380		
	.1670	1.7801	.0938	-2.366	406		
	.1720	1.8500	.0930	-2.375	404	410	39
	.1946	1.6811	.1157	-2.156	454		
	.1385	1.9330	.0716	-2.636	352		
	.2195	1.8211	.1205	-2.116	464		
EF 273	.1896	1.2824	.1478	-1.912	520 (5kb)		
	.2283	1.3672	.1670	-1.799	560		
	.2195	1.3250	.1657	-1.797	556	555	28
	.2095	1.1560	.1812	-1.708	585		
EF 736	.2570	1.6980	.1513	-1.888	531 (6kb)		
	.2780	1.445	.1924	-1.648	610		
	.2944	1.412	.2085	-1.568	640		
	.2977	1.675	.1777	-1.727	582		
	.2576	1.523	.1692	-1.777	566		
	.2590	1.246	.2078	-1.571	639		
	.2625	1.256	.2090	-1.565	641		
	.2938	1.4571	.2016	-1.6012	627	578	52
	.2676	1.722	.1554	-1.862	540		

## Mg/Fe partitioning between coexisting garnet (rim) and biotite

sample	(Mg/Fe) <sub>ga</sub>	(Mg/Fe) <sub>bi</sub>	K <sub>D</sub>	ln K <sub>D</sub>	T <sub>1</sub> <sup>*</sup>	$\bar{T}$	s. dev.
	.2566	1.709	.1501	-1.896	520		
	.2610	1.756	.1486	-1.906	572		
	.2637	1.7962	.1468	-1.918	522		
EF 853	.2957	1.8192	.1625	-1.817	531		
	.3253	1.6992	.1914	-1.653	585		
	.2951	1.9142	.1542	-1.870	515		
	.3058	1.7785	.1719	-1.761	552		
	.3032	1.7500	.1732	-1.753	551		
	.3047	1.6320	.1867	-1.678	576		
	.2620	1.4957	.1751	-1.742	550	566	33
	.2810	1.4960	.1878	-1.672	599		
	.2809	1.7440	.1610	-1.826	549		
	.2970	1.6145	.1839	-1.693	594		
	.2865	1.4250	.2010	-1.604	626		
EF 660	.1621	.8482	.1911	-1.654	606		
	.1620	.8370	.1937	-1.641	611		
	.1441	.8232	.1750	-1.743	577		
	.1536	.8972	.1712	-1.765	570		
	.1450	.9435	.1537	-1.873	535		
	.1576	.8931	.1765	-1.735	580		
	.1322	.6415	.2061	-1.579	636	605	44
	.1492	.6515	.2290	-1.474	678		
	.1408	.7822	.1800	-1.715	586		
	.1413	.6069	.2328	-1.457	685		
	.1621	.8482	.1911	-1.654	608		
	.1510	.8370	.1804	-1.712	587		
EF 876	.1634	1.0270	.1591	-1.838	546		
	.1790	1.0300	.1738	-1.750	575		
	.1223	.7390	.1655	-1.799	560		
	.1601	.7930	.2019	-1.600	628		
	.1646	.7921	.2070	-1.572	639		
	.1570	.6721	.2336	-1.454	687	604	42
	.1362	.6811	.1997	-1.611	624		
	.1273	.7130	.1785	-1.722	584		
	.1847	1.0335	.1787	-1.722	584		
	.2001	1.0280	.1946	-1.636	614		
EF 922 <sup>a</sup>	.2288	1.4910	.1534	-1.874	535		
	.2088	1.4417	.1448	-1.932	518		
	.2531	1.4481	.1748	-1.744	577		
	.2430	1.3350	.1820	-1.704	591		
	.2660	1.3971	.1904	-1.658	606	556	38
	.2650	1.444	.1835	-1.695	593		
	.1890	1.332	.1418	-1.953	512		
	.1960	1.3630	.1438	-1.939	518		
EF 870	.1173	.7340	.1597	-1.834	548		
	.1051	.6670	.1576	-1.848	543		
	.1337	.6630	.2016	-1.6012	626		
	.1533	.7696	.1992	-1.613	623		
	.1548	.8118	.1907	-1.657	607		
	.1203	.5908	.2036	-1.591	631	602	48
	.1186	.7200	.1647	-1.803	557		
	.1592	.7431	.2143	-1.540	651		
	.1431	.8616	.1661	-1.795	560		

## Mg/Fe partitioning between coexisting garnet (rim) and biotite

sample	(Mg/Fe) <sub>ga</sub>	(Mg/Fe) <sub>bi</sub>	K <sub>D</sub>	ln K <sub>D</sub>	T <sub>1</sub> <sup>*</sup>	$\bar{T}$	s.dev.
	.1427	.6215	.2296	-1.471	679		
EF 869	.1314	.9182	.1431	-1.944	514		
	.1313	.8601	.1528	-1.879	534		
	.1210	.8420	.1437	-1.939	516		
	.1256	.8699	.1444	-1.935	517		
	.1413	.9254	.1527	-1.879	534		
	.1277	.9253	.1380	-1.980	504		
	.0842	.8034	.1048	-2.255	434	513	30
	.1273	.8605	.1479	-1.911	524		
	.1355	.9279	.1460	-1.924	520		
	.1499	.9960	.1505	-1.894	529		
EF 922 <sub>b</sub>	.2451	1.2938	.1894	-1.664	604		
	.2316	1.5470	.1497	-1.899	528		
	.2809	1.3311	.2110	-1.556	644		
	.3154	1.6120	.1956	-1.631	616		
	.2670	1.4201	.1880	-1.671	602		
	.2431	1.3600	.1787	-1.722	584	604	42
	.2355	1.4008	.1681	-1.783	564		
	.2792	1.2612	.2213	-1.508	664		
	.2910	1.4420	.2018	-1.600	628		